Available online at www.sciencedirect.com
SCIENCE DIRECT
VIROLOGY
Virology 344 (2006) 541 – 559
www.elsevier.com/locate/yviro

Substitution of the transmembrane domain of Vpu in simian–human immunodeficiency virus ($SHIV_{KU1bMC33}$) with that of M2 of influenza A results in a virus that is sensitive to inhibitors of the M2 ion channel and is pathogenic for pig-tailed macaques

David R. Hout [a], Melissa L. Gomez [a], Erik Pacyniak [a], Lisa M. Gomez [a], Barbara Fegley [a], Ellyn R. Mulcahy [a], M. Sarah Hill [a], Nathan Culley [b], David M. Pinson [c], Warren Nothnick [d], Michael F. Powers [e], Scott W. Wong [e], Edward B. Stephens [a,*]

[a] *Department of Anatomy and Cell Biology, University of Kansas Medical Center, 3901 Rainbow Blvd., Kansas City, KS 66160, USA*
[b] *Laboratory Animal Resources, University of Kansas Medical Center, 3901 Rainbow Blvd., Kansas City, KS 66160, USA*
[c] *Department of Laboratory Medicine and Pathology, University of Kansas Medical Center, 3901 Rainbow Blvd., Kansas City, KS 66160, USA*
[d] *Department of Obstetrics and Gynecology, University of Kansas Medical Center, 3901 Rainbow Blvd., Kansas City, KS 66160, USA*
[e] *Vaccine and Gene Therapy Institute, Oregon National Primate Research Center, Oregon University for the Health Sciences, Beaverton, OR 97003, USA*

Received 23 May 2005; returned to author for revision 1 July 2005; accepted 1 August 2005
Available online 30 September 2005

Abstract

The Vpu protein of human immunodeficiency virus type 1 has been shown to shunt the CD4 receptor molecule to the proteasome for degradation and to enhance virus release from infected cells. The exact mechanism by which the Vpu protein enhances virus release is currently unknown but some investigators have shown that this function is associated with the transmembrane domain and potential ion channel properties. In this study, we determined if the transmembrane domain of Vpu could be functionally substituted with that of the prototypical viroporin, the M2 protein of influenza A virus. We constructed chimeric *vpu* gene in which the transmembrane domain of Vpu was replaced with that of the M2 protein of influenza. This chimeric *vpu* gene was substituted for the *vpu* gene in the genome of a pathogenic simian human immunodeficiency virus, $SHIV_{KU-1bMC33}$. The resulting virus, $SHIV_{M2}$, synthesized a Vpu protein that had a slightly different M_r compared to the parental $SHIV_{KU-1bMC33}$, reflecting the different sizes of the two Vpu proteins. The $SHIV_{M2}$ was shown to replicate with slightly reduced kinetics when compared to the parental $SHIV_{KU-1bMC33}$ but electron microscopy revealed that the site of maturation was similar to the parental virus $SHIV_{KU1bMC33}$. We show that the replication and spread of $SHIV_{M2}$ could be blocked with the antiviral drug rimantadine, which is known to target the M2 ion channel. Our results indicate a dose dependent inhibition of $SHIV_{M2}$ with 100 μM rimantadine resulting in a >95% decrease in p27 released into the culture medium. Rimantadine did not affect the replication of the parental $SHIV_{KU-1bMC33}$. Examination of $SHIV_{M2}$-infected cells treated with 50 μM rimantadine revealed numerous viral particles associated with the cell plasma membrane and within intracytoplasmic vesicles, which is similar to HIV-1 mutants lacking a functional *vpu*. To determine if $SHIV_{M2}$ was as pathogenic as the parental $SHIV_{KU-1bMC33}$ virus, two pig-tailed macaques were inoculated and followed for up to 8 months. Both pig-tailed macaques developed severe $CD4^+$ T cell loss within 1 month of inoculation, high viral loads, and histological lesions consistent with lymphoid depletion similar to the parental $SHIV_{KU-1bMC33}$. Taken together, these results indicate for the first time that the TM domain of the Vpu protein can be functionally substituted with the TM of M2 of influenza A virus, and shows that compounds that target the TM domain of Vpu protein of HIV-1 could serve as novel anti-HIV-1 drugs.

Keywords: Vpu; M2 protein; Viroporin; SHIV; Pathogenesis

Introduction

Human immunodeficiency virus type 1 (HIV-1) and several strains of simian immunodeficiency viruses (SIV) isolated from

* Corresponding author. Fax: +1 913 588 2710.
E-mail address: estephen@kumc.edu (E.B. Stephens).

0042-6822/$ - see front matter © 2005 Elsevier Inc. All rights reserved.
doi:10.1016/j.virol.2005.08.022

Fig. 1. Sequence of the proteins analyzed in this study. The (−) introduced in the Vpu_{M2} sequence was for purposes of sequence alignment.

non-human primates encode for a small membrane bound protein known as the Vpu protein (Strebel et al., 1988; Cohen et al., 1988; Huet et al., 1990; Barlow et al., 2003; Courgnaud et al., 2002; 2003). The Vpu protein from laboratory-adapted subtype B HIV-1 has been extensively studied with respect to its role in the virus life cycle and has resulted in the identification of two major functions in replication. The Vpu down-regulates the CD4 receptor in the rough endoplasmic reticulum (RER) and shunts it to the proteasome for degradation (Fujita et al., 1997; Schubert et al., 1998). Studies have shown that the highly conserved hinge region containing two casein kinase II sites is required for the CD4 degradation (Schubert et al., 1994; Paul and Jabbar, 1997) and other studies have shown that the predicted two α-helical domains within the cytoplasmic domain and sequences within the transmembrane (TM) domain are also required for efficient degradation of CD4 (Tiganos et al., 1998). Additionally, Vpu also enhances virus release from infected cells (Klimkait et al., 1990). Examination of cells infected with HIV-1 viruses containing large deletions within the *vpu* gene by electron microscopy revealed a different pattern of virus maturation with many particles tethered together at the cell surface and within intracellular vesicles. Some investigators have mapped Vpu-mediated virion release to the TM domain and other investigators have provided evidence that the TM domain forms an ion channel (Ewart et al., 1996; Schubert et al., 1996a). This evidence suggests that Vpu of HIV-1 is a member of a class of viral proteins known as the viroporins, which include the M2 protein of influenza A virus, the 6K protein of Sindbis virus (SV), and the 2B protein of poliovirus (Gonzalez and Carrasco, 2003).

In a previous study, evidence was provided that one viroporin could substitute for one another (Gonzalez and Carrasco, 2001).

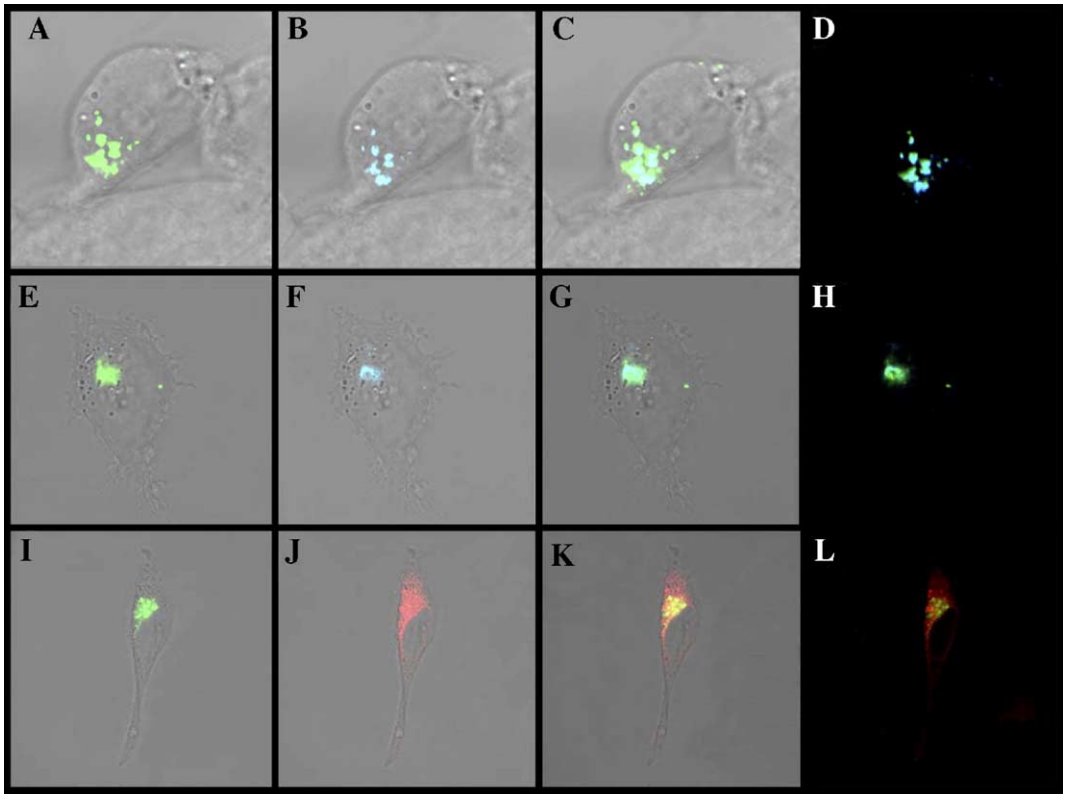

Fig. 2. Vpu_{M2}EGFP is expressed in the same intracellular compartments as the wild type Vpu. 293 cells were co-transfected with vectors expressing VpuEGFP or Vpu_{M2}EGFP and DsRed2-ER or ECFP-Golgi. At 48 h, cells expressing EGFP and DsRed2 or ECFP were identified and images collected using laser scanning confocal microscopy as described in the Materials and methods section. (A–D) 293 cells co-transfected with VpuEGFP and ECFP-Golgi. (A) Expression of VpuEGFP. (B) Expression of ECFP-Golgi. (C) Merge of panels A and B. (D) Fluorescence micrograph of EGFP and ECFP fusion proteins from panels A and B. (E–H) 293 cells co-transfected with Vpu_{M2}EGFP and ECFP-Golgi. (E) Expression of Vpu_{M2}EGFP. (F) Expression of ECFP-Golgi. (G) Merge of panels E and F. (H) Fluorescence micrograph of EGFP and ECFP fusion proteins from panels E and F. (I–L) 293 cells co-transfected with Vpu_{M2}EGFP and DsRed2-ER. (I) Expression of Vpu_{M2}EGFP. (J) Expression of DsRed2-ER. (K) Merge of panels I and J. (L) Fluorescence micrograph of EGFP and DsRed2 fusion proteins from panels I and J.

In this study, these investigators determined if the Vpu protein could substitute for the 6K protein of SV, which facilitates budding of virus particles and regulates transport of viral glycoproteins through the secretory pathway. Transfection of BHK cells with an SV vector that did not express the 6K protein, pSVDelta6K, resulted in lower membrane permeabilization, impaired glycoprotein processing, and deficient virion budding. These investigators showed that expression of Vpu protein under a duplicated late promoter (pSVDelta6KVpu) restored enhanced membrane permeability, normal glycoprotein precursor processing, and facilitated infectious virus particle production. Other studies have shown that derivatives of the Na^+ K^+ antiporter amlioride could inhibit the Vpu ion channel and decrease virus release from cells (Ewart et al., 2002, 2004).

Our laboratory has been using the chimeric simian human immunodeficiency/macaque model to study the role of Vpu and its various domains in $CD4^+$ T cell loss and pathogenesis (Stephens et al., 2002; Singh et al., 2003; Hout et al., 2004a, 2005). Using a pathogenic molecular clone known as $SHIV_{KU\text{-}1bMC33}$, we showed that the Vpu does indeed contribute to pathogenesis (Stephens et al., 2002). More recently, we have shown that the casein kinase II sites within the cytoplasmic domain and the TM domain of Vpu contribute to the pathogenicity of this virus (Singh et al., 2003; Hout et al., 2005). In this study, we constructed a simian–human immunodeficiency virus ($SHIV_{M2}$) mutant in which the transmembrane domain of Vpu was changed to the TM domain of the prototypical viroporin, the M2 protein of influenza A virus. Our results show that this chimeric Vpu was capable of down-regulating CD4 from the cell surface, that the replication of a virus was constructed with this chimeric protein ($SHIV_{M2}$) was sensitive to the effects of rimantadine, and that inoculation of pig-tailed macaques with the $SHIV_{M2}$ virus resulted in severe $CD4^+$ T cell loss and AIDS. These results show for the first time that the ion channel from the M2 protein (i.e., the TM domain of the M2 protein) and Vpu can be exchanged and suggests a "commonality" with respect to their involvement in virus maturation from cells. Finally, these results provide "proof of concept" that compounds that interact with and perturb the function of the TM domain of Vpu could represent a novel class of anti-HIV-1 drugs (Fig. 1).

Results

Expression of the Vpu_{M2}EGFP reveals a similar intracellular localization to the unmodified protein and is functional for CD4 down-modulation

We analyzed the intracellular transport of the Vpu_{M2} protein by fusion to the enhanced green fluorescent protein

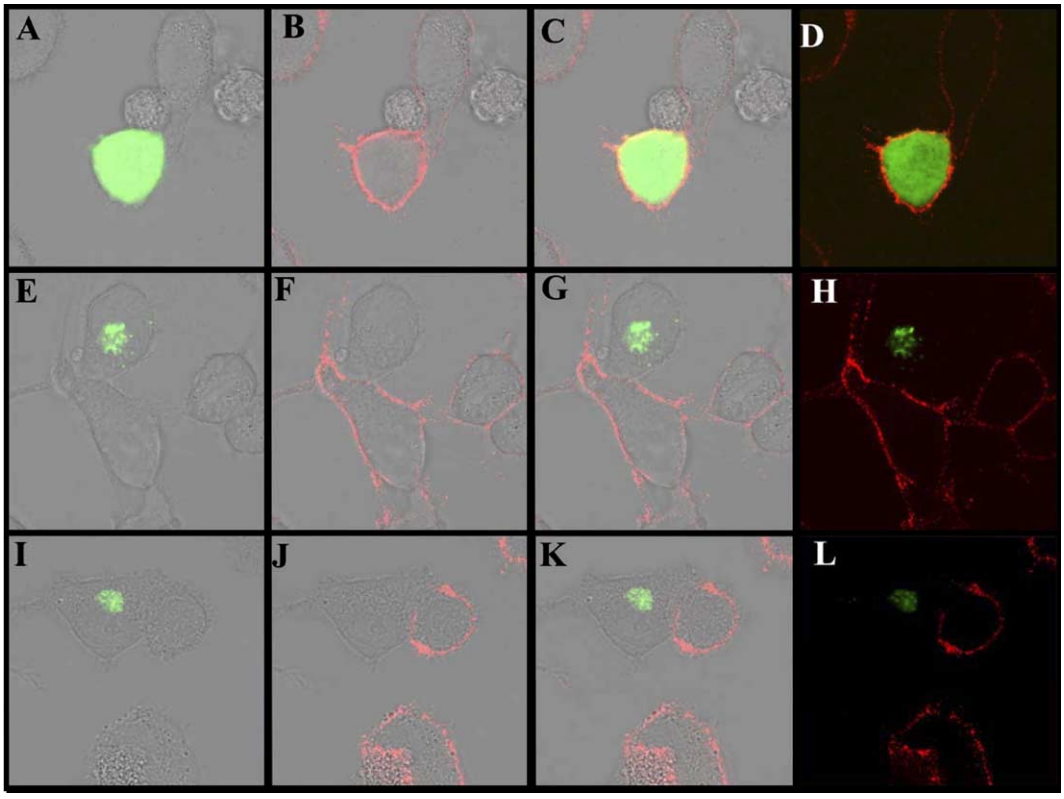

Fig. 3. CD4 down-regulation by EGFP, VpuEGFP, and Vpu_{M2}EGFP. HeLa $CD4^+$ cells, which express CD4, were transfected with vectors expressing EGFP, VpuEGFP, or Vpu_{M2}EGFP. At 48 h post-transfection, cells were stained for surface CD4 using α-CD4 antibody and a rhodamine conjugated secondary antibody followed by fixation with 1% formalin. Cells were examined by laser scanning confocal microscopy. (A, E, and I) Cells examined using a filter to visualize EGFP expression and layered onto a phase contrast image of the cell. (B, F, and J) Cells were examined using a filter to identify cell surface CD4 expression and layered onto a phase contrast image of the cells. (C, G, and K) Fluorescent micrographs merging EGFP and CD4 images. (A–D) Cells transfected with a vector expressing EGFP. (E–H) Cells transfected with a vector expressing VpuEGFP. (I–L) Cells transfected with a vector expressing Vpu_{M2}EGFP.

(EGFP) (Singh et al., 2003; Pacyniak et al., 2005). Co-transfection with the vectors expressing the unmodified subtype B protein (VpuEGFP) and ECFP-Golgi resulted in nearly complete co-localization (Figs. 2A–D). Co-transfection of 293 cells with the vectors expressing the unmodified subtype B Vpu protein (VpuEGFP) and DsRed2-ER resulted in this protein being partially co-localized with this intracellular markers (data shown; Gomez et al., 2005; Pacyniak et al., 2005). Co-transfection of 293 cells with vectors expressing Vpu_{M2}EGFP and DsRed2-ER resulted in partial localization of the Vpu_{M2}EGFP with the DsRed2-ER (Figs. 2E–H) and is similar to what we have previously shown for the unmodified VpuEGFP protein (Gomez et al., 2005; Pacyniak et al., 2005). Co-transfection of 293 cells with the vectors expressing Vpu_{M2}EGFP and ECFP-Golgi resulted in the two proteins being almost completely co-localized (Figs. 2I–L). Finally, we co-transfected cells with the vectors expressing Vpu_{M2}EGFP and ECFP-Mem. Similar to the unmodified VpuEGFP protein, the Vpu_{M2}EGFP did not appear to be expressed on the cell surface (data not shown). These results indicate that replacement of the Vpu TM domain with that of the M2 protein of influenza A virus still resulted in a protein that was transported to the same intracellular compartments as the unmodified Vpu protein and correlated well with our recent study that identified the cytoplasmic domain as having a Golgi retention signal (Pacyniak et al., 2005).

We determined if the Vpu_{M2}EGFP was capable of preventing cell surface expression of CD4. HeLa $CD4^+$ cells were transfected with vectors expressing EGFP, VpuEGFP, and Vpu_{M2}EGFP. At 48 h post-transfection, live cells were stained for cell surface CD4, fixed, and examined by confocal microscopy. As shown in Figs. 3A–D, cells expressing EGFP did not prevent cell surface CD4 expression while transfection of HeLa $CD4^+$ cells with a vector expressing VpuEGFP prevented cell surface expression (Figs. 3E–H), which is similar to what we previously reported (Pacyniak et al., 2005; Singh et al., 2003). Transfection of HeLa $CD4^+$ cells with the vector expressing Vpu_{M2}EGFP prevented cell surface expression of CD4 (Figs. 3I–L) and was similar to the unmodified VpuEGFP. In addition, we performed co-transfection experiments with vectors expressing EGFP, VpuEGFP, or Vpu_{M2}EGFP and human CD4. The results confirmed that the VpuEGFP and Vpu_{M2}EGFP induced CD4 degradation while CD4 was stably expressed in the presence of EGFP (data not shown). These results indicate that replacement of the Vpu TM domain with the TM from the M2 protein did not affect the ability of Vpu to induce degradation of CD4.

The $SHIV_{M2}$ virus encodes for a protein that has a slightly different M_r than the unmodified Vpu protein

We analyzed the expression of the Vpu protein in C8166 cultures inoculated with parental $SHIV_{KU\text{-}1bMC33}$ or $SHIV_{M2}$. $SHIV_{KU\text{-}1bMC33}$ expresses the unmodified, full length Vpu as well as the Tat, Rev, and Env proteins. The $SHIV_{M2}$ is the same as the $SHIV_{KU\text{-}1bMC33}$ virus except that the *vpu* gene was replaced with the chimeric *vpuM2* gene, which expresses a protein in which the transmembrane domain of Vpu has been replaced with the M2 protein of influenza A virus. Cultures were inoculated with equivalent amounts of virus and at 7 days post-inoculation, cells were radiolabeled and Vpu proteins immunoprecipitated from cell lysates. As shown in Fig. 4A, a protein with an M_r of 16,000 was immunoprecipitated from $SHIV_{KU\text{-}1bMC33}$-inoculated cultures. A Vpu protein was also immunoprecipitated from $SHIV_{M2}$-inoculated C8166 cultures with a slightly slower mobility in SDS-PAGE, which is probably a reflection of the structure of the Vpu_{M2} protein.

The $SHIV_{M2}$ virus replicates with kinetics that are slightly delayed compared to the parental $SHIV_{KU\text{-}1bMC33}$

We performed p27 growth curves to quantify the amount of virus released following inoculation of C8166 cells.

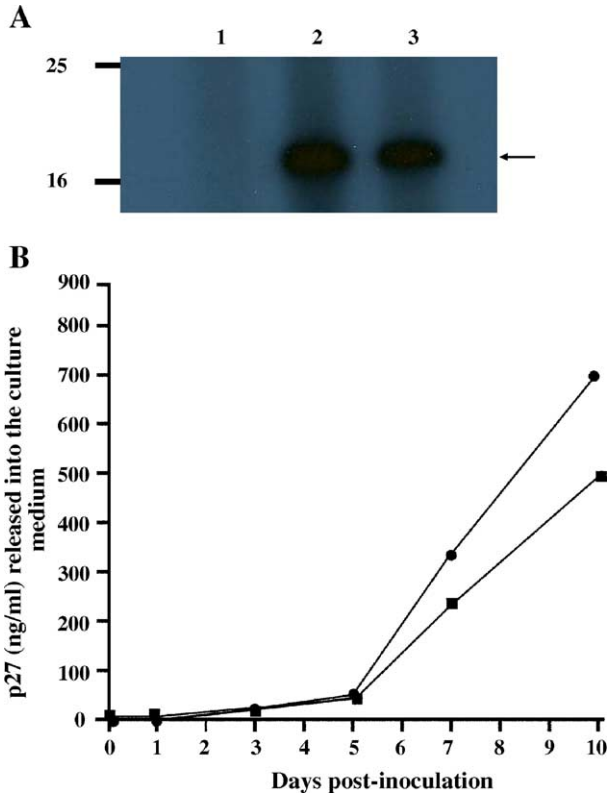

Fig. 4. Immunoprecipitation of Vpu proteins from $SHIV_{KU\text{-}1bMC33}$- and $SHIV_{M2}$-inoculated cultures and p27 growth curves. (A) C8166 cultures were inoculated with $SHIV_{KU\text{-}1bMC33}$ or $SHIV_{M2}$ at an MOI of approximately 0.01. Cultures were incubated for 6 days and then radiolabeled with ^{35}S-methionine/cysteine for 5 h. Vpu proteins were immunoprecipitated from cell lysates using an α-Vpu serum as described in the Materials and methods section. All samples were analyzed under reducing conditions by SDS-PAGE (12.5% gel) and visualized by standard autoradiographic techniques. Lane 1: Vpu proteins immunoprecipitated from uninoculated cultures. Lane 2: Vpu proteins immunoprecipitated from $SHIV_{M2}$-inoculated cultures. Lane 3: Vpu proteins immunoprecipitated from $SHIV_{KU\text{-}1bMC33}$-inoculated cultures. The location of the molecular weight markers is shown on the left. (B) Growth curves of $SHIV_{KU\text{-}1bMC33}$ (●) and $SHIV_{M2}$ (■) in C8166 cells. Cultures of C8166 cells were inoculated with either $SHIV_{KU\text{-}1bMC33}$ or $SHIV_{M2}$ as described in the text. Aliquots of the culture medium were assayed for the presence of p27 antigen. The growth curves were performed in duplicate with the mean value shown.

Cultures were inoculated with an equivalent dose of infectious units of $SHIV_{KU\text{-}1bMC33}$, $SHIV_{TM}$, or $SHIV_{M2}$ as determined by titration in the HOS-CXCR4 cell line. Culture fluids were collected at 0, 1, 3, 5, 7, and 10 days post-inoculation and assayed for p27 released into the culture medium. As shown in Fig. 4B, growth curves revealed slightly reduced kinetics of viral p27 released into the culture medium when compared to the parental $SHIV_{KU\text{-}1bMC33}$. We also compared the synthesis and processing of the $SHIV_{KU\text{-}1bMC33}$ or $SHIV_{M2}$ viral proteins by pulse-chase analyses. Our results indicated that the $SHIV_{M2}$ viral proteins were processed similarly to those of the parental $SHIV_{KU\text{-}1bMC33}$ virus (data not shown).

The $SHIV_{M2}$ virus has a maturation pattern that is similar to the parental $SHIV_{KU\text{-}1bMC33}$ in C8166 cells

Since the p27 assays indicated that the $SHIV_{M2}$-inoculated cultures released less virus into the culture medium with time, we examined cultures inoculated with $SHIV_{M2}$ and parental $SHIV_{KU\text{-}1bMC33}$ at 7 days post-inoculation by electron microscopy to determine if the pattern of maturation was different among the two viruses. As shown in Fig. 5A, $SHIV_{KU\text{-}1bMC33}$-inoculated C8166 cells revealed viral particles maturing at the cell plasma membrane. The mean number of virus particles associated with 100 infected cells was 47.8 (Fig. 6A). Examination of $SHIV_{M2}$-inoculated cultures by electron microscopy also revealed virus maturing at the cell plasma membrane (Fig. 5C) with a mean number of 40 viral particles associated per cell (Fig. 6B), which was not statistically different from the parental virus. We did not observe $SHIV_{M2}$ maturing into intracellular vesicles as we previously described for other SHIVs with Vpu mutants, $SHIV_{TM}$, or $SHIV_{Vpenv}$ (Hout et al., 2004b, 2005).

The $SHIV_{M2}$ virus is sensitive to an inhibitor that blocks the M2 ion channel

As the above results of the pulse-chase analyses and electron microscopy suggested that the kinetics of viral release from cells were slightly reduced for $SHIV_{M2}$ when compared

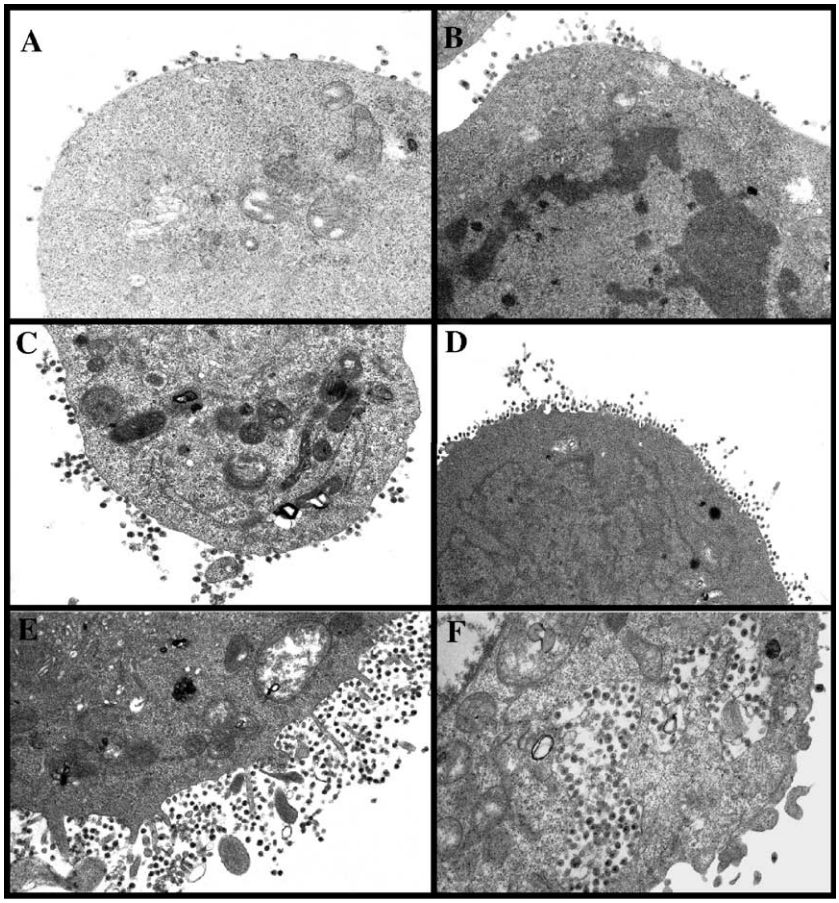

Fig. 5. Electron microscopy examination of C8166 cells inoculated with $SHIV_{KU\text{-}1bMC33}$ or $SHIV_{M2}$ in the absence or presence of rimantadine. C8166 cells were inoculated with either $SHIV_{M2}$ or $SHIV_{KU\text{-}1bMC33}$ for 7 days. Cells were washed three times with PBS and processed for electron microscopy as described in the Materials and methods section. (A) Untreated C8166 cells inoculated with parental $SHIV_{KU\text{-}1bMC33}$. (B) C8166 cells inoculated with parental $SHIV_{KU\text{-}1bMC33}$ treated with 50 μM rimantadine. (C) Untreated C8166 cells inoculated with $SHIV_{M2}$. (D) C8166 cells inoculated with parental $SHIV_{M2}$ in the presence of 50 μM rimantadine. (E) C8166 cells inoculated with parental $SHIV_{M2}$ in the presence of 50 μM rimantadine. (F) C8166 cells inoculated with parental $SHIV_{M2}$ in the presence of 50 μM rimantadine.

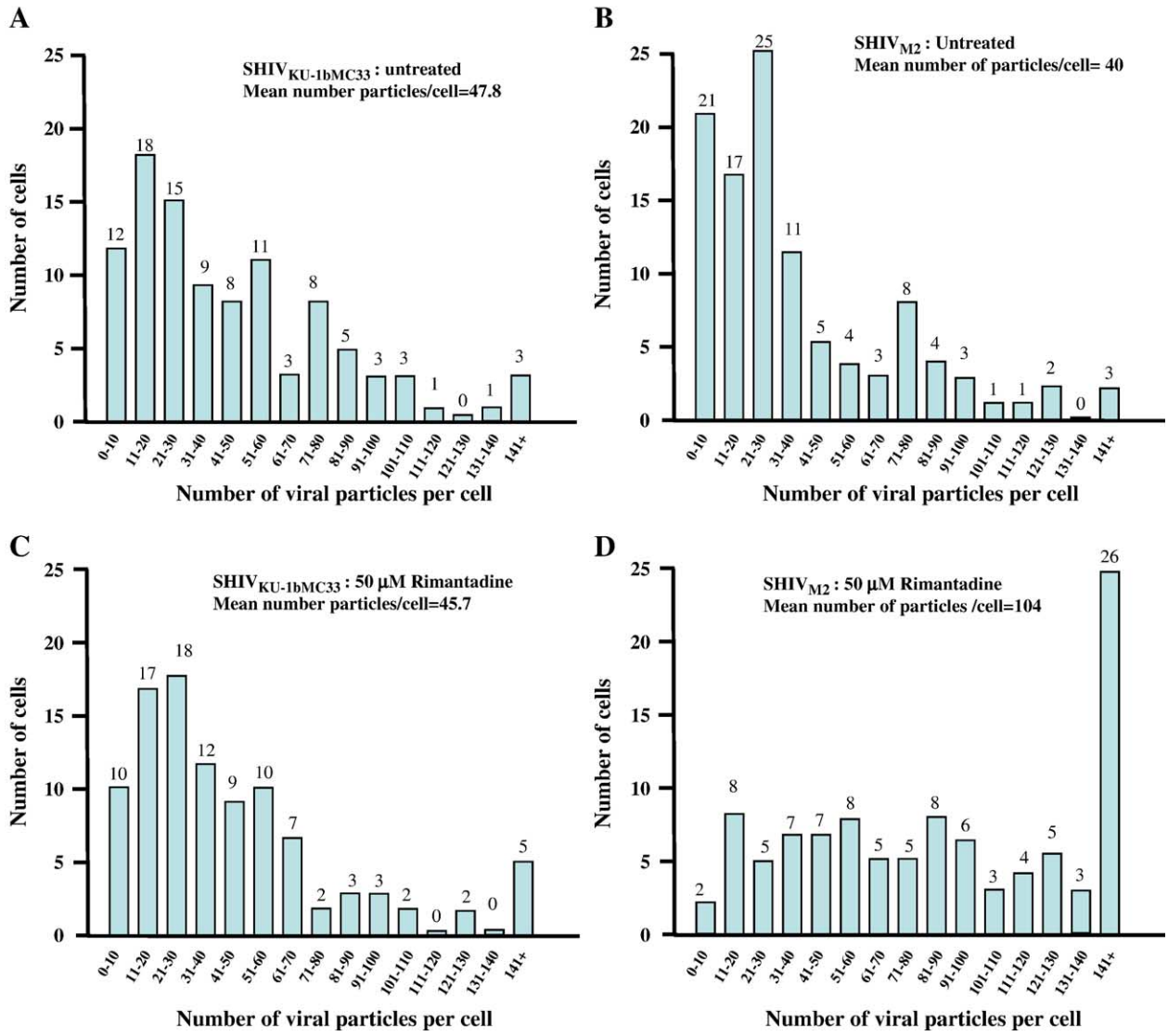

Fig. 6. Enumeration of viral particles associated with the infected C8166 cells following inoculation with $SHIV_{KU-1bMC33}$ (A, C) or $SHIV_{M2}$ (B, D) in the absence (A, B) or presence of 50 μM rimantadine. Cells were inoculated with equivalent doses of infectious virus and at 7 days processed for electron microscopy as described in the Material and methods section. The number of viral particles associated with ≥100 cells per virus/treatment was enumerated. (A) The distribution of the number of viral particles per cell following inoculation with $SHIV_{KU-1bMC33}$. (B) The distribution of the number of viral particles per cell following inoculation with $SHIV_{M2}$. (C) The distribution of the number of viral particles per cell following inoculation with $SHIV_{KU-1bMC33}$ and treatment with 50 μM rimantadine. (D) The distribution of the number of viral particles per cell following inoculation with $SHIV_{M2}$ and treatment with 50 μM rimantadine. The mean number of particles per cell for each virus/treatment is shown at the top of each panel.

to parental $SHIV_{KU-1bMC33}$, we determined if $SHIV_{M2}$ was sensitive to inhibitors (amantadine and rimantadine), which are known to interact with and block the ion channel of the M2 protein (Hay et al., 1986). We first assessed the toxicity of the amantadine and rimantadine in C8166 cells. Cells were incubated with 100 μM, 10 μM, 1 μM, or with no rimantadine or amantadine and the number of viable cells assessed by the trypan blue dye exclusion method at 0, 1, 3, and 7 days. Amantadine was found to be somewhat toxic at 100 μM while rimantadine was not toxic at a concentration of 100 μM (data not shown). Due to this apparent toxicity associated with 100 μM amantadine, we chose to work with rimantadine. C8166 cells were inoculated with either the parental $SHIV_{KU-1bMC33}$ virus or $SHIV_{M2}$ for 4 h, the inoculum removed, and then incubated for 7 days in medium containing various concentrations of rimantadine (100 μM, 75 μM, 50 μM, 25 μM, or untreated). At 7 days, the culture supernatants were collected and assayed for p27 levels. As shown in Fig. 7A, rimantadine reduced virus release by an average of >99% at 100 μM, 90% at 75 μM, 63% at 50 μM, and 14% at a 25 μM. At 10 μM, rimantadine had no effect on p27 release (data not shown). Rimantadine had no effect on the replication of $SHIV_{KU-1bMC33}$ in C8166 cultures at any of the tested concentrations (Fig. 7A). We confirmed the p27 results by radiolabeling infected cells at 7 days post-inoculation with ^{35}S-methionine/cysteine for 12 h. The culture supernatants were recovered and cell lysates prepared after the 12 h pulse-labeling and used for immunoprecipitations using an anti-SHIV serum. As shown in Fig. 7B,

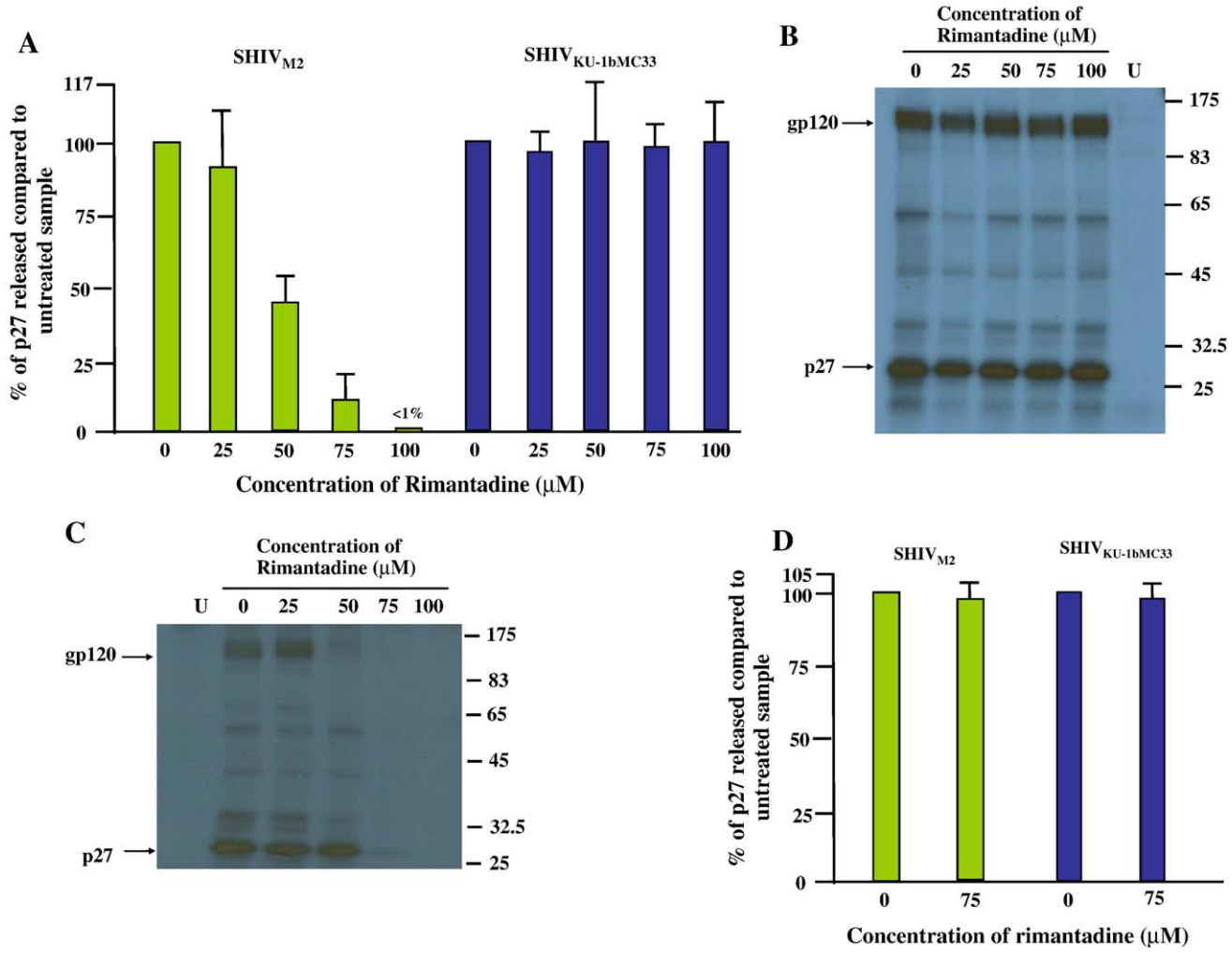

Fig. 7. Rimantadine, an inhibitor of the M2 ion channel, inhibits the replication of SHIV$_{M2}$ but not parental SHIV$_{KU-1bMC33}$. (A) C8166 cells were inoculated with either SHIV$_{M2}$ or SHIV$_{KU-1bMC33}$ in the presence of various concentrations of rimantadine or in the absence of rimantadine. At 7 days post-inoculation, culture supernatants were removed, clarified, and assayed for the presence of p27 antigen. (B, C) At 7 days post-inoculation, untreated or treated cells were starved for methionine and cysteine and radiolabeled overnight with ^{35}S-methionine/cysteine for 12 h. Viral proteins were immunoprecipitated from the culture medium as described in the Materials and Methods section from SHIV$_{KU-1bMC33}$ (B) or SHIV$_{M2}$ (C). (D) C8166 cells were treated with 50 μM rimantadine for 1 h prior to and during the initial 4 h inoculation period. The inoculum and rimantadine were removed, cells washed three times, and cultures refed with fresh medium lacking rimantadine. At 7 days post-inoculation, culture medium was collected and assayed for p27 antigen using antigen capture assays. The p27 assay experiments were repeated three times and the immunoprecipitations two times.

none of the concentrations of rimantadine effected the release of the parental SHIV$_{KU-1bMC33}$ viral proteins into the culture medium. In contrast, the levels of SHIV$_{M2}$ viral proteins released into the culture medium were reduced in a dose dependent manner from SHIV$_{M2}$-inoculated cultures in the presence of 50 μM to 100 μM rimantadine (Fig. 7C). Thus, the immunoprecipitation results correlated with the p27 assays. Taken together, our results indicate that substitution of the Vpu transmembrane domain with that of the M2 protein from influenza A virus resulted in a SHIV that was sensitive to the effects of the M2 channel blocker, rimantadine.

In the above experiments, virus was allowed to enter susceptible cells for 4 h prior to treatment with rimantadine. We next determined if the rimantadine would interfere with entry into the susceptible cells. For this experiment, C8166 cells were inoculated with SHIV$_{M2}$ virus in the presence of 75 μM rimantadine for 4 h. At 4 h, the virus inoculum and rimantadine were removed, the cells washed three times, and then incubated in fresh medium lacking rimantadine for 7 days. As shown in Fig. 7D, treatment of cells with rimantadine prior to and during the 4 h inoculation period had no effect on the virus replication, indicating that entry was not effected by the rimantadine.

Electron microscopy reveals an increase in the accumulation of viral particles at the cell plasma membrane of SHIV$_{M2}$-infected cells treated with rimantadine

As the inhibitor studies indicated that rimantadine inhibited the replication of the virus, we examined the maturation of the SHIV$_{M2}$ and parental SHIV$_{KU-1bMC33}$ in the presence of 50 μM rimantadine. We chose to examine infected cells treated with 50 μM rimantadine as this concentration that exhibited (~45%) inhibition of SHIV$_{M2}$

release as determined by p27 assays. As shown in Fig. 5B, the maturation of parental $SHIV_{KU\text{-}1bMC33}$ in C8166 cells treated with 50 μM rimantadine was comparable to untreated cultures with a mean number of viral particles per cell being 45.7. Electron microscopy revealed that the mean number of viral particles per cell was 40 with the majority of the cells having less than 50 viral particles per cell (Fig. 6C). In contrast, the maturation of $SHIV_{M2}$ was considerably altered in the presence of rimantadine. As shown in Figs. 5D–E, virus particles appeared to accumulate at the cell surface of cells with a mean number of viral particles per cell of 104, which was approximately 2.5 times that observed for the untreated cells (Fig. 6D). The difference in the number of particles per cell in untreated and 50 μM treated $SHIV_{M2}$-infected cultures was significant ($P < 0.001$). Electron microscopy also revealed that particles appeared to be tethered to the membrane and could be observed maturing within intracellular vesicles (Fig. 5F). These results suggested that $SHIV_{M2}$ release from infected cells was reduced in the presence of 50 μM rimantadine.

The $SHIV_{M2}$ infects pig-tailed macaques and causes a rapid $CD4^+$ T cell loss observed with the parental $SHIV_{KU\text{-}1bMC33}$

To assess whether $SHIV_{M2}$ was capable of causing $CD4^+$ T cell loss in macaques, two pig-tailed macaques (CW8F, CW8H) were inoculated with $SHIV_{M2}$. $CD4^+$ T cell counts and viral loads were then monitored for up to 40 weeks (Fig. 8A). After inoculation with $SHIV_{M2}$, the circulating $CD4^+$ T cell numbers in macaque CW8F dropped from 2865 cells/μl at 1 week post-inoculation to 83 cells/μl at 4 weeks post-inoculation. The circulating $CD4^+$ T cells in the this macaque continued to remain low (<100 cells/μl) until the macaque was euthanized at 24 weeks (circulating $CD4^+$ T cells at 54 cells/μl) in moribund condition. Similar to macaque CW8F, macaque CW8H had a high level of circulating $CD4^+$ T cells at 1 week post-inoculation (2318 cells/μl), which dropped to less than 100 cells/μl by 6 weeks post-inoculation. Macaque CW8H was euthanized at 40 weeks post-inoculation ($CD4^+$ T cell level at 63 cells/μl) in a moribund condition. The circulating $CD4^+$ T cell levels were similar to those observed following inoculation of macaques with parental $SHIV_{KU\text{-}1bMC33}$, in which there was a severe drop in the levels of circulating $CD4^+$ T cells within 4 weeks post-inoculation (Fig. 8B) but were in contrast to those observed following inoculation with $SHIV_{TM}$ (Hout et al., 2005).

The plasma viral loads in animals inoculated with $SHIV_{M2}$ were similar to parental $SHIV_{KU\text{-}1bMC33}$

We compared the plasma viral loads in the three macaques inoculated with $SHIV_{M2}$ with the viral loads in macaques inoculated with the parental $SHIV_{KU\text{-}1bMC33}$. As shown in Figs. 9A–B, both macaques inoculated with $SHIV_{M2}$ had viral loads that were similar to those from macaques inoculated with the parental $SHIV_{KU\text{-}1bMC33}$.

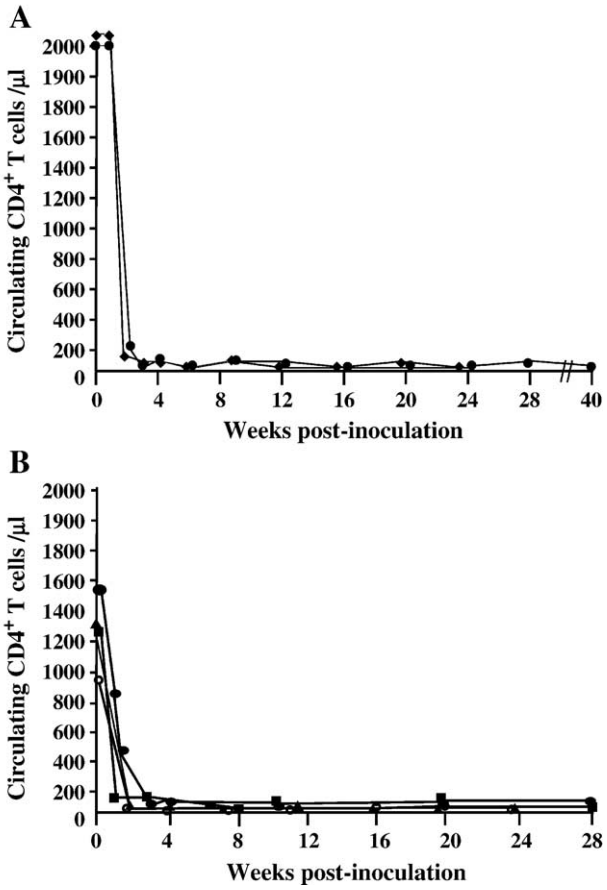

Fig. 8. Macaques inoculated with $SHIV_{M2}$ develop $CD4^+$ T cell loss within 1 month of inoculation. (A) Macaques CW8H (●) and CW8F (♦) were inoculated with $SHIV_{M2}$ and circulating $CD4^+$ T cells determined at various times post-inoculation. (B) Circulating $CD4^+$ T cell levels in macaques 2000 (●), 2001 (■), CM4G (○), and CM4K (▲) determined at various times post-inoculation with parental $SHIV_{KU\text{-}1bMC33}$.

The sequence of the vpu gene was stable during the period of severe $CD4^+$ T cell loss

In order to assess the stability of the *vpu* gene during the course of infection, DNA was extracted from PBMC samples at 2, 6, 12, 20 weeks, and at necropsy. The *vpu* sequence was amplified and directly sequenced and compared to the input *vpu* sequence of the $SHIV_{M2}$. As shown in Fig. 10, the *vpu* (and in particular, the sequence of the TM domain) was stable in the *vpu* sequences amplified through 20 weeks. At the 24 weeks and at necropsy, a termination codon was detected in the *vpu* sequences amplified from the PBMC DNA isolated from macaque CW8H, which resulted in a truncation of the predicted Vpu protein to 22 amino acids. We also analyzed the *vpu* sequences analyzed from the mesenteric lymph node, spleen, and thymus at necropsy. Sequence analysis of the *vpu* sequences amplified from isolated mesenteric lymph node and spleen DNA from CW8H also had a termination codon in the same position detected in the PBMC while the *vpu* sequences amplified from the thymus DNA were identical to the input virus. The *vpu* sequences amplified from isolated spleen, mesenteric

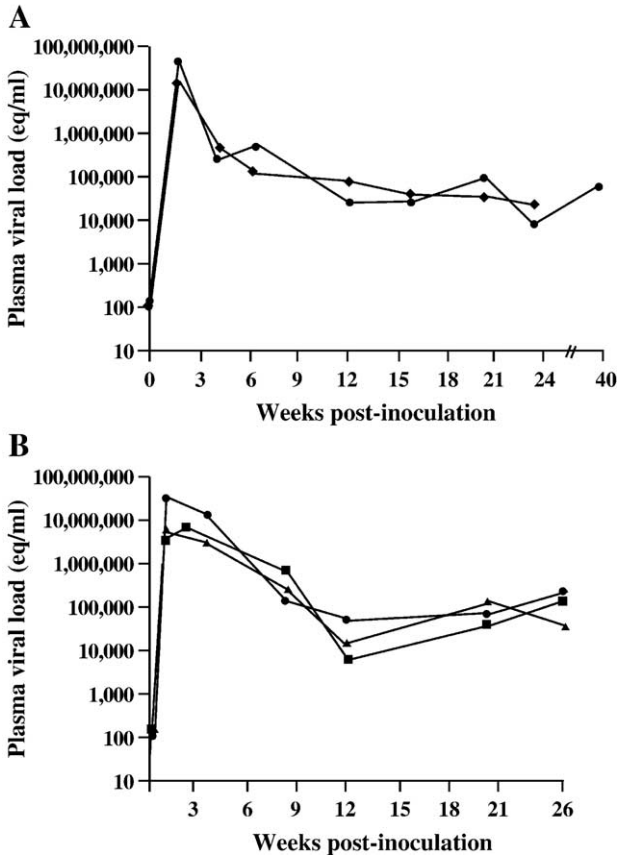

Fig. 9. Plasma viral loads in macaques inoculated with $SHIV_{M2}$ and $SHIV_{KU\text{-}1bMC33}$. (A) Plasma viral loads in macaques CW8H (●) and CW8F (♦) inoculated with $SHIV_{M2}$. (B) Plasma viral RNA levels in three macaques (2000, ●; 2001, ■; and CM4K, ▲) inoculated with $SHIV_{KU\text{-}1bMC33}$. Samples were subjected to real-time RT-PCR and Taqman probe homologous to the SIV *gag* gene. Standard curves were generated using five dilutions of viral RNA of known concentration.

lymph node, and thymus DNA from macaque CW8F had no sequence changes.

Isolation of a highly cytopathic virus from the spleen of macaque CW8H with a truncated Vpu protein

Sequence analysis indicated that the sequence of the Vpu_{M2} protein was truncated starting at 24 weeks post-inoculation. While performing infectious centers assays at necropsy, we observed co-culturing isolated spleen cells from CW8H with the indicator C8166 cell line resulted in massive syncytial cytopathology that occurred within 1–2 days post-inoculation with the C8166 cells. Cell-free supernatants from these cultures were harvested and a series of three limiting dilution assays using C8166 cells were performed to isolate this strain of virus. In each of assay, the massive syncytial cytopathology was again observed. As shown in Fig. 11, this syncytial cytopathology was easily visible within 24 h after inoculation of cultures, which was significantly faster when compared to $SHIV_{M2}$-inoculated where syncytia formation usually occurs at approximately 5 days post-inoculation (Fig. 11). DNA was isolated from cells of the passaged virus and the sequence of the *vpu* and gp120 region of *env* determined. Sequence analysis of the *vpu* gene revealed a mutation that resulted in a truncated Vpu protein of 22 amino acids with the UGG codon being mutated to a UAG (Fig. 10A). Based on this sequence, we predicted that this virus isolate would be resistant to the actions of rimantadine. The CW8H spleen virus was grown in C8166 cells in the presence or absence of 100 μM rimantadine. Our results indicated that the CW8H spleen virus was resistant to the actions of rimantadine (data not shown). Sequence changes in the Env are also known to affect the syncytial nature of HIV-1 and SIV. Thus, we also analyzed the sequence of the gp120 region of *env* by sequencing the amplified gp120 sequences from the virus-infected cells. The results indicated 10 amino acid substitutions in the gp120 when compared to the parental $SHIV_{KU\text{-}1bMC33}$ (Fig. 10B). Among the amino acid substitutions observed in the $SHIV_{CW8HSPL}$ were the elimination of two N-linked glycosylation sites.

Macaques inoculated with $SHIV_{M2}$ developed histopathology that was similar to the macaques inoculated with parental $SHIV_{KU\text{-}1bMC33}$

We examined the histological sections from tissues of macaques at necropsy and compared the lesions to those observed following inoculation with parental $SHIV_{KU\text{-}1bMC33}$. No significant histological lesions were observed in the 15 regions of the CNS, the heart, liver, lungs, kidney, or pancreas. As shown in Fig. 12, the $SHIV_{M2}$-inoculated macaques developed severe atrophy of the thymus and lymph nodes demonstrated little follicular activity and no germinal centers. The distribution of virus in the various visceral organs was determined by PCR for viral 2-LTR sequences. As shown in Table 1, viral 2-LTR sequences were detected in DNA isolated from 5 of 13 visceral organs from CW8F, and 7 of 13 visceral organs tissues from CW8H. The majority of the tissue DNAs that were positive for the presence of 2-LTR sequences were the lymphoid organs. We also analyzed the DNA samples isolated from 15 regions of the CNS for *gag* and 2-LTR sequences (Table 1). Macaques CW8F and CW8H were positive for *gag* sequences in 11 of 15 and 10 of 15 regions of the CNS, respectively (data not shown). However, only one region from macaque CW8F (cerebellum) was positive for 2-LTR sequences and none from macaque CW8H (Table 1).

Analysis of viral loads by PCR-ICA is shown in Fig. 13 and indicates that the viral loads in the $SHIV_{M2}$-inoculated macaques were comparable to macaques inoculated with $SHIV_{KU\text{-}1bMC33}$. The results correlate well with plasma viral load data, $CD4^+$ T cell loss, and histopathology.

Discussion

The Vpu protein of HIV-1 has two established functions in virus replication and these include the down-regulation of CD4 from the cell surface and enhancement of virion release from infected cells. While the molecular mechanisms of the CD4 down-regulation have been determined, much less is known

about the enhancement of virion release from cells. Enhanced virion release has been associated with the TM domain of the Vpu protein and some investigators have shown that the TM domain is capable of forming an ion channel (Ewart et al., 1996; Schubert et al., 1996a). Expression of Vpu in frog oocytes results in a conductance that is weakly selective for cations and modeling studies have suggested that a pentameric structure for the Vpu TM domain would be optimal for the formation of such a channel (Grice et al., 1997; Sansom et al., 1998; Wray et al., 1999; Cordes et al., 2001, 2002; Lopez et al., 2002). Recently, the structure of the Vpu transmembrane domain was elucidated by synthesizing the hydrophobic transmembrane domain along with 12 hydrophilic cytoplasmic residues for stability and solubility (Park et al., 2003). Thus, the

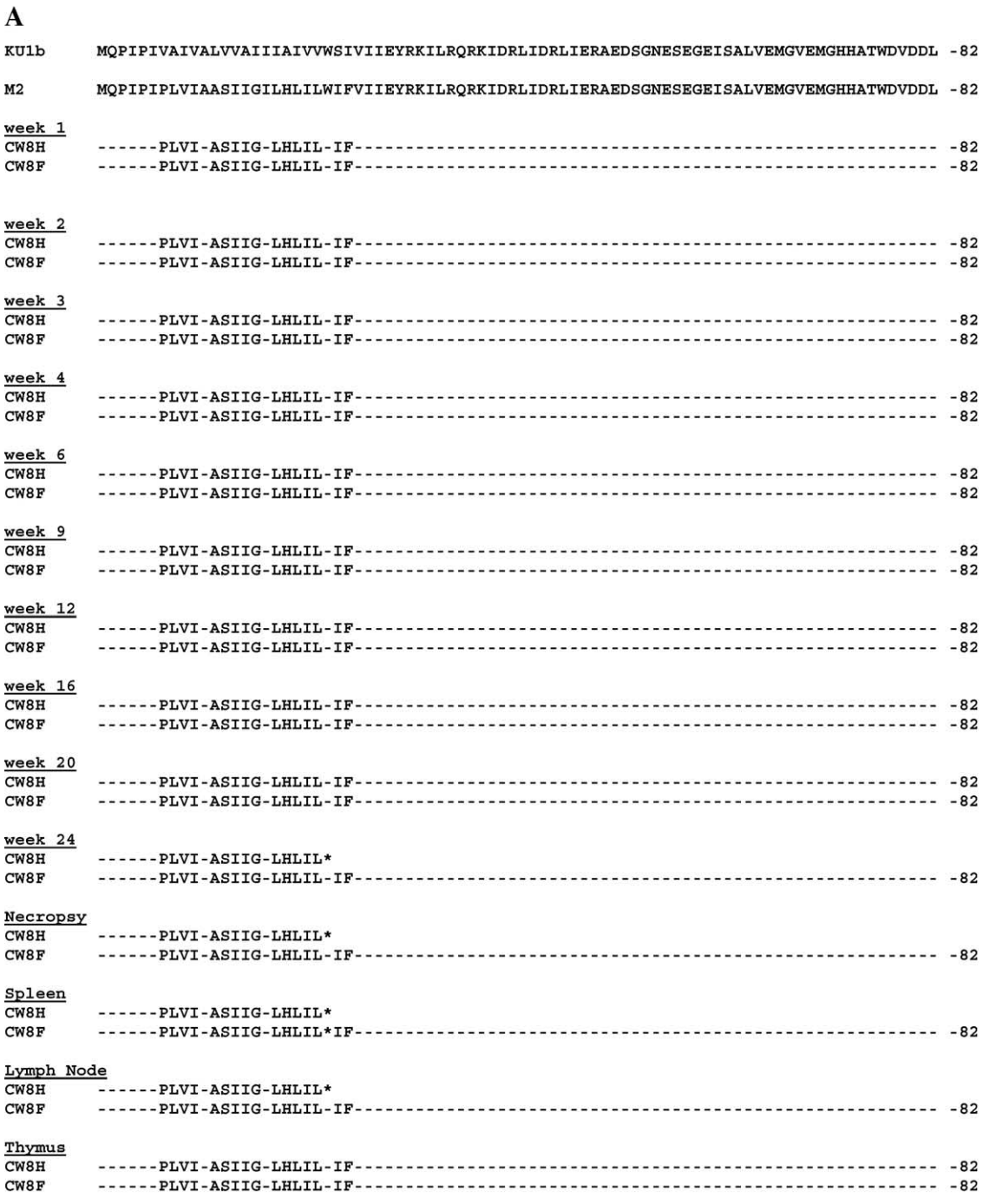

Fig. 10. Sequence analysis of the *vpu* and *env* genes amplified from macaques inoculated with $SHIV_{M2}$. (A) DNA was isolated from PBMC of macaques at various times post-inoculation, and from the spleen, mesenteric lymph nodes and thymus at necropsy. The *vpu* gene was amplified, isolated, and sequenced. Shown at the top are the sequence of the parental $SHIV_{KU\text{-}1bMC33}$ and $SHIV_{M2}$. (*) denotes the presence of a termination codon resulting in a truncated Vpu sequence. (B) Comparison of the predicted amino acid sequences of the gp120 region of Env from parental $SHIV_{KU\text{-}1bMC33}$ and the virus isolated from the spleen tissue of macaque CW8H ($SHIV_{CW8HSPL}$). The horizontal lines under the sequences indicate the two N-linked glycosylation sites that were eliminated in the $SHIV_{CW8HSPL}$ virus.

B

```
Ku1b-   MRVKEKYQHLWRWGWRWGTMLLGMLMICSATEKLWVTVYYGVPVWKEATTTLFCASDAKAYDTEVHNVWATHACVPTDPSPQEVVLVNVTENFNMWKNDM  -100
CW8H-   ----------------------------------------------------------------------------------------------------

Ku1b-   VEQMHEDIISLWDQSLKPCVKLTPLCVSLNCTDLKNDTNTNSSSGGMIMEKGEIKNCSFNISTSIRGKVQKEYALLYKLDIIPIDNDTTSYTLTSCNTSV  -200
CW8H-   ----------------------------------------K--R---------------------------------H----------------D---

Ku1b-   ISQACPKVSFEPIPIHYCAPAGFAILKCNNKTFNGTGPCTNVSTVQCTHGIRPVVSTQLLLNGSLAEEEVVIRSVNFMDNAKTIIVQLNTSVEINCTRPG  -300
CW8H-   ----------------------------------------------------------------------------------------------------

Ku1b-   NNTIKRIRIHRGPGRAFVTMGKIGNMRQAHCNISRAKWDNTLKQIASKLREQFGNNKTIIFKQSSGGDPEIVTHSFNCGGEFFYCNSTQLFNSTWFNSTG  -400
CW8H-   ----------------------------------------------T----G-----------------------------------------------N--

Ku1b-   STEGSNNTEGSDTITLPCRIKQIINMWQKVGKAMYAPPISGQIRCLSNVTGLLLTRDGGNGNNESEIFRPGGGDMRDNWRSELYKYKVVKIEPLGIAPTK  -500
CW8H-   --------K---------K--------------------------------------K-------------------------------------

Ku1b-   AKRRVVQREKRA  -512
CW8H-   ------------
```

Fig. 10 (*continued*).

available evidence suggests that the Vpu protein of HIV-1 is a member of a class of proteins known as the viroporins.

Previous studies showed that two derivatives of the Na^+ K^+ antiporter amiloride, dimethyl amiloride (DMA) and hexamethylene amiloride (HMA), inhibited Vpu-mediated virion release and replication in macrophages (Ewart et al., 2002, 2004). In the most recent study, both DMA and HMA were shown to inhibit HIV-1 replication in monocyte-derived macrophage cultures (Ewart et al., 2004). While these studies are encouraging that compounds targeting the Vpu function can reduce virus replication, it is not yet clear whether these compounds directly target the Vpu protein or if they target another cellular function used by Vpu. Furthermore, both DMA and HMA have a "narrow window of efficacy" before

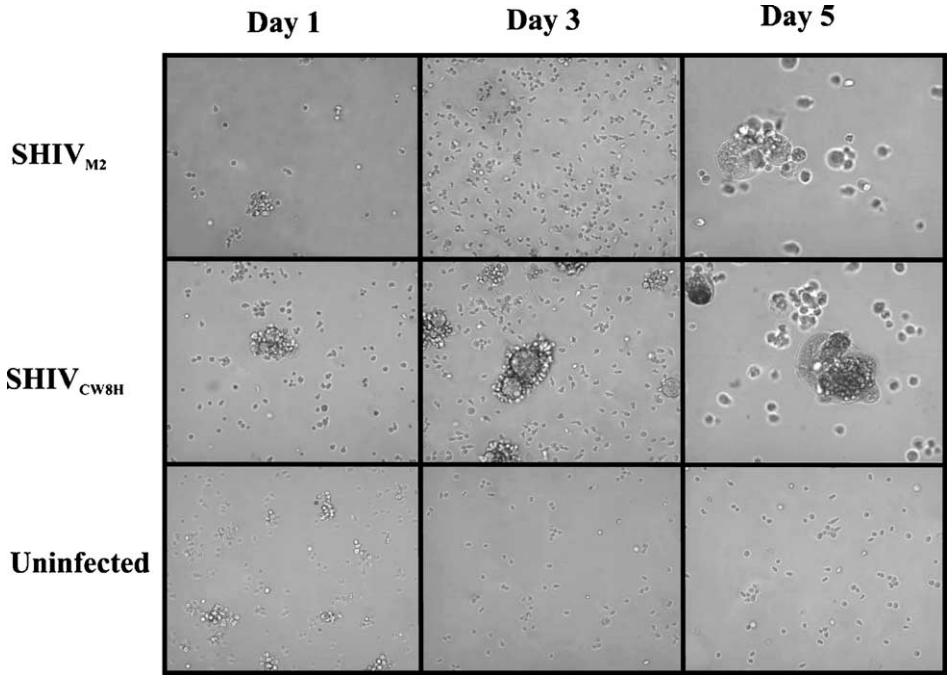

Fig. 11. Phase contrast micrographs of a highly cytopathic variant from the spleen of macaque CW8H that was resistant to rimantadine. (Upper row) Phase contrast micrographs of C8166 cells inoculated with SHIV$_{M2}$ at 1, 3, or 6 days post-inoculation. (Middle row) Phase contrast micrographs of C8166 cells inoculated with SHIV$_{CW8H}$ at 1, 3, or 6 days post-inoculation. (Bottom row) Phase contrast micrographs of mock-inoculated C8166 cells at 1, 3, or 6 days.

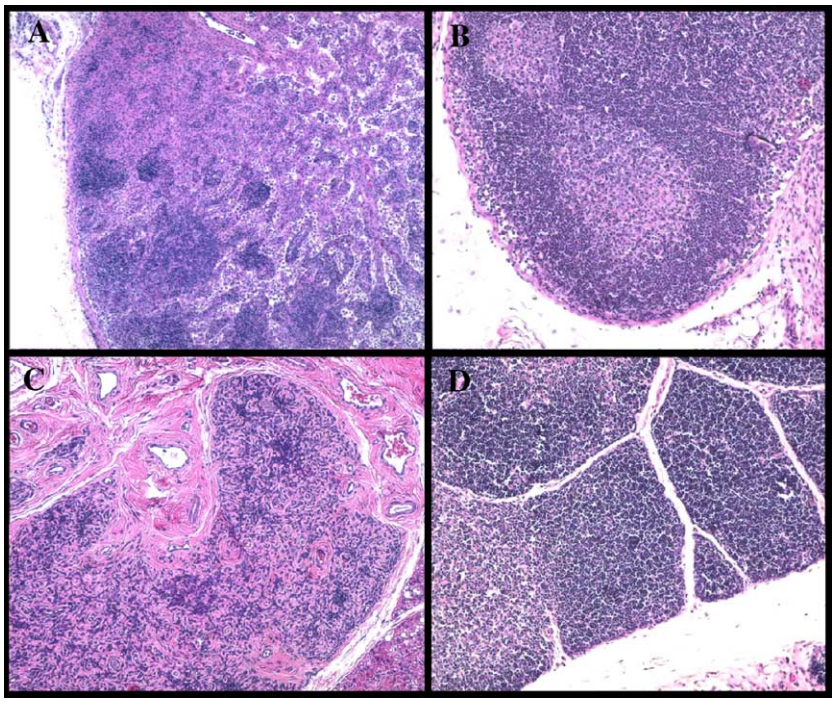

Fig. 12. Pathology associated with $SHIV_{M2}$ infection. Hematoxylin and eosin stains of sections from the mesenteric lymph node (A, B), and thymus (C, D) from macaque CW8F (A, C) and an uninoculated macaque (B, D).

they become cytotoxic. In this study, we determined if another viroporin could substitute for the Vpu TM and if drugs directly targeting this TM domain could interfere in virus replication. We chose to insert the M2 protein ion channel because the structure of the Vpu protein has been modeled after the well studied M2 protein of influenza A virus (Lamb and Pinto, 1997; Grice et al., 1997; Sansom et al., 1998; Fischer and Sansom, 2002; Gonzalez and Carrasco, 2003). These two proteins are similar in their length, orientation in the membrane, and ability to form oligomeric structures in membranes. The M2 protein of influenza virus has two important functions in the influenza A virus replication cycle (Gonzalez and Carrasco, 2003). During virus entry by receptor-mediated endocytosis, acidification of endosomes activates the M2 ion channel resulting in the influx of H^+ into the virus resulting in a low pH conformational change in the hemaglutinin (HA). This results in exposure of the fusion peptide domain of the HA, fusion of the endosomal and viral membranes, and release of the viral nucleocapsids into the cytoplasm. In addition to its role in virus entry, the M2 protein is important for transport of the HA molecule to the cell surface. As there is a gradual drop in the pH from the rough endoplasmic reticulum (RER) to the trans-Golgi network (TGN), the M2 protein (based on its orientation) becomes activated and causes an efflux of H^+ from the TGN, thereby preventing a low pH conformational change of the newly synthesized HA molecule as it transported to the cell surface (Sakaguchi et al., 1996; Henkel and Weisz, 1998; Henkel et al., 1999). Finally, there are two well established antiviral drugs, amantadine and rimantadine, that target the M2 ion channel and have been used to treat influenza A virus infections in humans.

We chose to insert the gene for this chimeric Vpu_{M2} protein into the genetic background of the pathogenic molecular clone $SHIV_{KU\text{-}1bMC33}$ in order to analyze its role in disease caused by SHIV. Using this pathogenic molecular clone, we recently reported on the construction of a SHIV in which the amino acids of TM domain of Vpu were scrambled but kept the hydrophobic nature of this domain (Hout et al., 2005). When $SHIV_{TM}$ was inoculated into three pig-tailed macaques, none developed the severe $CD4^+$ T cell loss or high viral burdens that are normally observed following inoculation with the parental $SHIV_{KU\text{-}1bMC33}$ (Hout et al., 2005). Additionally, the $SHIV_{TM}$ replicated poorly in C8166 cells and had a maturation pattern that was differed from the parental $SHIV_{KU\text{-}1bMC33}$ (Hout et al., 2005). The results of electron microscopy studies indicated that $SHIV_{M2}$ had a maturation pattern that was similar to that of parental $SHIV_{KU\text{-}1bMC33}$ (Hout et al., 2005). Furthermore, unlike $SHIV_{TM}$, $SHIV_{M2}$ was pathogenic in pig-tailed macaques with both developing severe $CD4^+$ T cell loss within 1 month and histological lesions in lymphoid tissues, which was similar to the parental $SHIV_{KU\text{-}1bMC33}$ virus. Together, these data indicate that the $SHIV_{M2}$ was phenotypically different from $SHIV_{TM}$.

We showed that the Vpu_{M2} chimeric protein was stable during the period of severe $CD4^+$ T cell depletion with no nucleotide substitutions occurring in *vpu* amplified from PBMC or lymphoid organs from macaque CW8F at necropsy. However, we did observe that beginning at 24 weeks the amplified *vpu* had a termination codon that truncated the Vpu protein. Sequence analysis revealed that this became the predominant genotype in all three lymphoid organs analyzed. The termination codon occurred at codon 22 (the UGG was changed to a UAG) that normally encodes for a tryptophan

Table 1
Distribution of viral 2LTR sequences in tissues from macaques inoculated with SHIVM2[a]

Tissue	Macaque	
	CW8F	CW8H
Visceral organs		
Heart	(−)	(−)
Kidney	(−)	(−)
Liver	(−)	(+)
Lung	(−)	(+)
Pancreas	(−)	(+)
Salivary gland	(−)	(−)
Axillary lymph node	(−)	(−)
Inguinal lymph node	(+)	(−)
Mesenteric lymph node	(+)	(+)
Small intestine	(+)	(+)
Spleen	(+)	(+)
Tonsil	(−)	(−)
Thymus	(+)	(+)
CNS		
Frontal cortex	(−)	(−)
Motor cortex	(−)	(−)
Parietal cortex	(−)	(−)
Occipital cortex	(−)	(−)
Temporal cortex	(−)	(−)
Cerebellum	(+)	(−)
Medulla	(−)	(−)
Pons	(−)	(−)
Midbrain	(−)	(−)
Thalamus	(−)	(−)
Corpus callosum	(−)	(−)
Basal ganglia	(−)	(−)
Cervical spinal cord	(−)	(−)
Thoracic spinal cord	(−)	(−)
Lumbar spinal cord	(−)	(−)

[a] Tissue DNA samples were analyzed for 2-LTR sequences using nested DNA PCR as described in the text.

residue. Interestingly, the M2 protein ion channel is thought to act through the interaction of a histidine and tryptophan residues in the motif His-X-X-X-Trp with the tryptophan residue of this motif serving as the gate of the M2 proton channel (Okada et al., 2001; Takeuchi et al., 2003; Tang et al., 2002; Wang et al., 1995). Thus, in the $SHIV_{CW8HSP}$ virus, the gate of the ion channel was effectively eliminated and suggesting that if stably expressed in membranes that this proton channel might be constitutively open. Alternatively, the M2 ion channel might be effectively eliminated suggesting that there was a selection against a virus with a functional M2 ion channel. Additionally, this virus gained the phenotypic property of being extremely fusogenic, with cell-free stocks causing syncytia formation in C8166 cultures within 24 h post-inoculation. Previous studies have reported that the Vpu negative viruses result in enhanced syncytia formation (Yao et al., 1993). Furthermore, other investigators have identified determinants in the envelope glycoprotein that resulted in increased fusogenicity in pathogenic SHIV-KB9 (Etemad-Moghadam et al., 2000). It will be of interest to determine if the truncation of the Vpu or the amino acid substitutions within the gp120 region of Env contributes to this enhanced fusogenicity of this virus isolate.

As these results suggest that the function imparted by the TM domain of Vpu can be substituted with the same region from the M2 protein of influenza A virus, the obvious question that arises is "How does the M2 TM positively affect the maturation of the SHIV?" The finding that rimantadine did not affect virus production when used at the early stages of virus entry suggests that the M2 protein is probably exerting its effects at the level of virus maturation. Previous studies have shown that the TM domain of the Vpu protein is involved in the enhanced release function (Klimkait et al., 1990; Schubert et al., 1996b). One possibility is that the structure of these two TM domains may have more "commonality" than previously envisioned. It is quite possible that the M2 TM with its ion channel properties may modify the local environment that is conducive for the maturation of this SHIV from cells. Finally, electron microscopic examination of $SHIV_{M2}$-infected cells that were treated with 50 μM rimantadine, a concentration that reduced release of viral p27 by approximately 50%, revealed an accumulation of viral particles at the cell plasma membrane and within intracellular vesicles. The finding that a 50 μM concentration rimantadine caused an alteration in the virus maturation pattern that was similar to that reported for Vpu (−) HIV-1 suggests that the M2 ion channel may be acting through a similar mechanism as the TM of the native Vpu. Taken together, these data provide evidence that the chimeric Vpu_{M2} protein was active and that inhibitors targeting the M2 ion channel could reduce release of $SHIV_{M2}$ from infected cells. As $SHIV_{M2}$ was inhibited by rimantadine, it will be of interest to determine if administration of rimantadine to macaques can reduce viral loads and disease. If successful, it would provide direct in vivo evidence that the Vpu protein and specifically the TM domain of the Vpu protein are novel targets for anti-HIV-1 drugs.

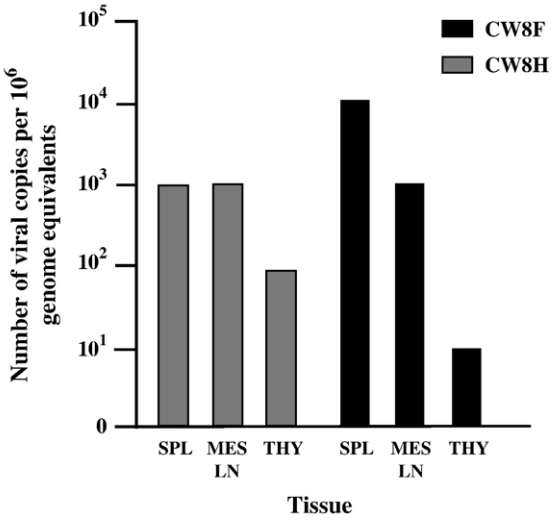

Fig. 13. Virus loads in tissues from macaques inoculated with $SHIV_{KU\text{-}1bMC33}$ and $SHIV_{M2}$. Cells were isolated from the mesenteric lymph nodes (MES LN), spleen (SPL), and thymus (THY) and analyzed for the number of viral genome copies per 10^6 cells as described in the Materials and methods section.

Materials and methods

Cells, plasmids, and viruses

The lymphocyte C8166 cell line was used for transfections as well as indicator cells to measure infectivity and cytopathicity of the viruses used in this study. C8166 cells were maintained in RPMI-1640, supplemented with 10 mM HEPES buffer pH 7.3, 2 mM glutamine, 5 μg per ml gentamicin, and 10% fetal bovine serum (R10FBS). The derivation of $SHIV_{KU\text{-}1bMC33}$ has been previously described (McCormick-Davis et al., 2000; Stephens et al., 2002). The construction and characterization have been previously described (Hout et al., 2005). The plasmids expressing the subtype B Vpu fused to the EGFP (pc*vpu*EGFP) have been previously described (Singh et al., 2003; Gomez et al., 2005; Pacyniak et al., 2005). Subcellular marker plasmids used in these studies include DsRed2-ER (catalog number 632409; fusion of the targeting signal of calreticulin), pECFP-Golgi (catalog number 632357; fusion with Golgi resident protein β 1,4 galactosyltransferase), and pECFP-Mem (catalog number 632360; fusion of the N-terminal 20 amino acids of neuromodulin or GAP-43, which has a palmityolation signal), which were obtained from Clontech (Palo Alto, Ca). The ECFP-Mem is a marker for membranes including the cell plasma membrane.

Construction of the $SHIV_{M2}$

A virus $SHIV_{M2}$ was constructed in which the TM sequence of Vpu (VAIVALVVAIIIAIVVWSI) was replaced with the TM sequence (PLVIAASIIGILHLILWIF) from the M2 protein of influenza A virus in the parental $SHIV_{KU\text{-}1bMC33}$. Plasmid pUC19ΔSNvpu12, containing the *Sph*I to *Kpn*I fragment of $SHIV_{KU\text{-}1bMC33}$ in pUC-19 (and coding for the *tat*, *rev*, *vpu*, and 5′ end of *env*) was used for the site-directed mutagenesis studies of the Vpu TM. The plasmid used was pUC19ΔSNvpu12 and the Quick-Change Mutagenesis Kit (Stratagene) according to the manufacturer's instructions. A total of 17 site-directed mutagenesis reactions were performed to alter the Vpu TM sequence to the that of the M2 protein. Clones were isolated, plasmids isolated, and the entire insert sequenced to determine if the mutations were introduced as expected and to ensure that no additional changes were introduced during the mutagenesis step. The plasmid, designated as pUC19ΔSNvpuM2, was digested to completion with *Sph*I and *Kpn*I, the 450 base pair insert isolated and ligated into p3′$SHIV_{KU1\text{-}bMC33}$ using T4 DNA ligase, which was also digested with *Kpn*I and *Sph*I and gel purified. The resulting plasmid, p3′$SHIV_{M2}$, was sequenced to insure that no insertions or deletions had occurred during the cloning process. The $SHIV_{M2}$ virus was generated by digestion of p5′-SHIV-4 and p3′$SHIV_{M2}$ with *Sph*I, ligation of the two plasmids together with T4 DNA ligase, and transfection into C8166 cells as previously described (McCormick-Davis et al., 2000; Stephens et al., 2002; Hout et al., 2004a, 2005). Stocks of virus were prepared and stored at −86 °C.

Construction of Vpu_{M2}EGFP

In order to assess the intracellular transport of the Vpu_{M2} and its ability to down-regulate CD4 expression, we constructed an expression vector in which the Vpu_{M2} was fused to the gene for EGFP using the same methodology as we used to express the subtype B, C proteins of HIV-1 as well as four SIV_{cpz} Vpu proteins (Singh et al., 2003; Pacyniak et al., 2005; Gomez et al., 2005; Hout et al., 2005).

Transfections and laser scanning confocal fluorescence microscopy analysis

Plasmids expressing VpuEGFP and other fusion proteins were transfected in human 293 cells to assess their subcellular localization using a cationic polymer (polyethylenimine) transfection reagent (ExGen 500, MBI Fermentas) using the manufacturer's protocol. Briefly, $1-3 \times 10^5$ cells were seeded onto cover slips in each well of a 6 well tissue culture plate 24 h prior to transfection. Transfection was carried out on cultures that were 50–60% confluent using 4.75 μg plasmid DNA and 15.5 μl of ExGen 500 corresponding to 6 equivalents. Each plasmid DNA sample was diluted in 300 μl of 150 mM sodium chloride solution separately. Samples were vortexed gently and immediately centrifuged at low revolution for a few seconds. Polyethylenimine was then added to the plasmid DNA solution, mixed with a vortex, and allowed to stand at room temperature for 10 min. The 293 cells were washed with serum-free media twice and 3.0 ml of serum-free DMEM was added. Polyethylenimine/DNA mixture was added to the cells and the plate swirled by slow hand rotation for a couple of seconds. Culture plates were centrifuged at 280 × *g* for 5 min and incubated at 37 °C for 30 min. The medium from transfected cultures was replaced with fresh complete growth media and cells were incubated at 37 °C in 5% CO_2 atmosphere. Transfected cells were observed by confocal microscopy, which is known to have the advantage that fluorescence can be detected from cells in different optical sections. Transfected cells were grown in 35 mm Petri dishes, and were prepared for confocal microscopy as follows. Cells were rinsed briefly in phosphate buffered saline (PBS, pH 7.2) at room temperature. The cells were fixed in freshly prepared, ice cold, 1% paraformaldehyde in 0.13 M in sodium phosphate pH 7.2 for 2 min. The fixative was removed and the cells briefly rinsed in phosphate buffered saline. The saline was removed, and one drop of mounting media was placed on each dish. The mounting media are composed of 75% glycerol, 25% 0.13 M sodium phosphate buffer pH 8.0 plus 0.02% *n*-propyl gallate. A square number one glass cover slip was placed over each dish. The cells were imaged with a Zeiss LSM 510 confocal microscope in the upright configuration. The objective used was a 63 × 1.4 n.a. Plan Apochromat. Images were captured at 12 bit resolution with a pixel array of 1024 × 1024 and a zoom of 2.0×. The signal was averaged 4 times per line. The EGFP was excited with light at 488 nm (laser intensity 75% for all images), and the emitted light was collected after passing through a 505 nm

long pass filter. The amplifier offset and gain were identical for all images. The detector gain was decreased from 692 nm to 618 nm for cells expressing Vpu_{SC}EGFP1 since the intensity of the signal resulted in saturation. A Z stack of 20 optical slices was obtained so that the entire cell was imaged from bottom to top. The pinhole was set to 96 μm which at this wavelength represents one airy unit. The optical section had a width of 0.7 μm. Simultaneous to the acquisition of the confocal signal from the EGFP, a non-confocal transmitted light image was obtained to provide a reference point for the EGFP signal. Individual confocal slices were overlaid onto the greyscale transmitted light image.

To confirm the presence of the Vpu fusion protein at different subcellular compartments, a series of co-transfection studies were performed using vectors expressing either an ER marker fused to the fluorescent protein DsRed2 (pDsRed2-ER), a Golgi complex marker fused to a cyano-variant of EGFP(pECFP-Golgi), or a membrane marker (pECFP-Mem). 293 cells were co-transfected with vectors expressing the various Vpu fusion proteins and either DsRed2-ER, ECFP-Golgi, or ECFP-Mem. At 48 h post-transfection, cells were processed for confocal microscopy as described above, and cells identified expressing both proteins. Fluorescent digital images were obtained using a Zeiss LSM510 confocal microscope equipped with an Argon/2 laser (25 mW) for the excitation (488 nm, 50% laser power) and detection (band pass 505–530 nm filter; BP505-530) of EGFP, for the excitation (458 nm, 100% laser power) and detection (band pass 475–525 nm filter; BP475-525) of ECFP, and for excitation (558 nm, 100% laser power) and detection (band pass 583 nm filter; LP560) of DsRed2. Images were acquired in Multitrack channel mode (sequential excitation/emission) with LSM510 (v 3.2) software and a Plan-Apochromat 100×/1.4 Oil DIC objective with frame size of 2048 × 2048 pixels. Detector gain was set initially to cover the full range of all the samples and background corrected by setting the amplifier gain, and all images were then collected under the same photomultiplier detector conditions and pinhole diameter.

Assays for detection of cell surface CD4 and degradation of CD4

To determine if the Vpu_{M2}EGFP construct was capable of promoting degradation of CD4 in transfected cells, we employed HeLa $CD4^+$ cells. Cultures of HeLa $CD4^+$ in which approximately 80–85% of the cells stained positive for surface CD4 were recloned to obtain a population of cells in which >99% of the cells stained positive for cell surface CD4. Briefly, HeLa $CD4^+$ cells were grown on cover slips and transfected with pc*vpu*EGFP as described earlier. At 48 h post-transfection, cells were washed twice with wash buffer (PBS pH 7.2, containing 2% fetal calf serum and 0.01% NaN_3) and reacted with mouse anti-CD4 (clone SFCI12T4D11CD4, Beckman-Coulter, 1:500 dilution) for 45 min. After the incubation, cover slips were washed three times and incubated with rhodamine-conjugated secondary antibody (goat anti-mouse, Chemicon, 1:50 dilution) for 35 min followed by washing five times in buffer without serum. Cells were then fixed in 1% formalin for 10 min, washed twice, equilibrated with anti-fade buffer, and mounted on microscope glass slides using Anti-fade (Molecular Probes, Oregon). Cells were immediately observed under a laser scanning confocal microscopy with appropriate filters for visualization of EGFP and CD4 staining. All the staining procedures were performed on ice and in the dark. HeLa $CD4^+$ cells transfected with EGFP alone served as control for down-regulation of CD4 and cultures of HeLa $CD4^+$ cells treated with wash buffer instead of primary antibody served as negative control for CD4 staining. A minimum of 400 EGFP expressing cells were counted.

In addition to detection of CD4 on the cell surface of transfected HeLa $CD4^+$ cells, co-transfection experiments were performed using vectors expressing each VpuEGFP fusion protein and a vector expressing the human CD4 protein (pCMV4Neo; Goldsmith et al., 1995). Cells were transfected with Vpu fusion and pCMV4Neo vectors at a 3:1 ratio, respectively. This was to insure that all cells transfected with the CD4 expressing vector were also transfected with the vector expressing the Vpu fusion proteins. At 48 h post-transfection, cells were starved for methionine and then radiolabled with 500 μCi ^{35}S-methionine/cysteine for 1 h. The radiolabel was removed and chased with 100× cold methionine/cysteine for 4 h. Cells were lysed in RIPA buffer, lysates prepared, and the CD4 immune precipitated using a rabbit anti-CD4 (sc-7219; Santa Cruz Biotechnology) and protein A Sepharose (PAS). Immune precipitates were collected, washed three times with 1× RIPA, and analyzed by SDS-PAGE (10% gel). Controls included co-transfection with pcEGFP (expressing on EGFP) as negative control for CD4 degradation and co-transfection with a pc*vpu*EGFP (expressing the subtype B VpuEGFP fusion protein) as a positive control for CD4 degradation.

Immunoprecipitation of Vpu proteins

To determine if Vpu proteins were expressed in $SHIV_{M2}$-inoculated cultures, C8166 cells were inoculated with 10^3 $TCID_{50}$ of either $SHIV_{M2}$ or $SHIV_{KU\text{-}1bMC33}$. At 5 days post-infection, the medium was removed and infected cells were incubated in methionine/cysteine-free Dulbecco's modified Eagle's medium (DMEM) for 2 h. The cells were then radiolabeled for 12 h with 500 μCi per ml of ^{35}S-Translabel (methionine and cysteine, ICN Biomedical, Costa Mesa, CA). Vpu proteins were immunoprecipitated from the cell lysates using an anti-Vpu serum as described previously (McCormick-Davis et al., 2000; Singh et al., 2003) prior to incubation with antiserum. Lysates were centrifuged in a microfuge to remove nuclei prior to the addition of antibody. Cell lysates were incubated with antibody for 16 h at 4 °C and immunoprecipitates were collected on protein A Sepharose. The beads were washed three times with RIPA buffer, and the samples were resuspended in sample reducing buffer and boiled. Proteins were analyzed by SDS-PAGE and visualized by standard autoradiographic techniques.

Pulse-chase analysis of viral proteins

To analyze the viral proteins synthesized and released from cells, C8166 cells were inoculated with 10^4 $TCID_{50}$ of either $SHIV_{M2}$ or $SHIV_{KU\text{-}1bMC33}$. At 7 days post-inoculation, the medium was removed and infected cells were incubated in methionine/cysteine-free Dulbecco's modified Eagle's medium (DMEM) for 2 h. The cells were then radiolabeled for 30 min with 1 mCi per ml of ^{35}S-Translabel (methionine and cysteine, ICN Biomedical, Costa Mesa, CA) and the radiolabel chased for various periods of time in DMEM containing 100× unlabeled methionine/cysteine. SHIV proteins were immunoprecipitated from the cell culture medium and infected cell lysates using plasma pooled from several rhesus monkeys infected previously with non-pathogenic SHIV-4. Briefly, the cell culture medium was clarified (16,000 × *g*) for 2 min. The supernatant was transferred and made 1× with respect to cell lysis buffer (50 mM Tris–HCl, pH 7.5; 50 mM NaCl; 0.5% deoxycholate; 0.2% SDS; 10 mM EDTA) and SHIV proteins were immunoprecipitated with 10 μl of a pooled serum from several monkeys that were inoculated with non-pathogenic SHIV for over 1 year. For immunoprecipitation of cell associated SHIV proteins, cell lysates were prepared as described previously (Stephens et al., 1995, 1997; McCormick-Davis et al., 2000; Hout et al., 2004a, 2005) prior to incubation with antiserum. Lysates were centrifuged in a microfuge to remove nuclei prior to the addition of antibody. Cell lysates and culture medium were incubated with antibody for 16 h at 4 °C. All immunoprecipitates were collected on protein A Sepharose, the beads washed three times with RIPA buffer, and the samples resuspended in sample reducing buffer. Samples were boiled and the SHIV specific proteins analyzed by SDS-PAGE. Proteins were then visualized by standard autoradiographic techniques.

p27 assays

p27 growth curves assays were used to assess replication kinetics of the $SHIV_{M2}$ or parental $SHIV_{KU\text{-}1bMC33}$. Cultures of 10^6 C8166 cells were inoculated with equivalent amounts (10 ng) of cell-free virus stocks for 2 h. At the end of 2 h, the cells were centrifuged at 400 × *g* for 10 min and the pellet washed with 10 ml of medium. This was repeated two additional times. The cells were resuspended in RPMI-1640 supplemented with 10% FBS and antibiotics and this was considered the 0 time point of the assay. Cultures were incubated at 37 °C and aliquots of the culture were removed at 0, 1, 3, 5, 7, and 10 days. The culture medium was separated from the cells by centrifugation and the culture supernatants assayed for p27 according to the manufacturer's instructions. For assays involving rimantadine, the drug was freshly prepared in RPMI-1640 medium as 10 mM stocks and filter sterilized prior to addition to cultures. Drug was added to cultures at the 0, 3, and 6 day time points.

Electron microscopy

To determine the site of intracellular maturation, infected cells were examined by electron microscopy. Cultures of C8166 cells were inoculated with $SHIV_{KU\text{-}1bMC33}$ or $SHIV_{M2}$ at a multiplicity of infection of 0.01. Cells were incubated for 7 days at which time cells were pelleted at 400 × *g* for 10 min. Cells were washed three times with 10 ml of phosphate buffered saline (pH7.4) and then fixed in 2% glutaraldehyde overnight at 4 °C. Cells were post-fixed in 1% osmium tetroxide (OsO4) for 1 h. The cells were washed twice with water and dehydrated through a series of alcohols (30–100%) followed by embedding in Embed 812 resin. Thin sections were cut at 80 A, stained with uranyl acetate and lead citrate, and examined under a JEOL 100CXII transmission electron microscope. The number of virus particles associated with 100 infected cells (either at the surface or within the cell) was enumerated. Data were analyzed by planned comparisons using unpaired *t* test. Data from the untreated and 50 μM treated $SHIV_{M2}$-infected cultures or $SHIV_{KU\text{-}1bMC33}$-infected cultures were compared.

Macaques analyzed in this study

Two 1–1.5 year old pig-tailed macaques (*Macaca nemestrina*; CW8F, CW8H) were inoculated intravenously with 1 ml of undiluted supernatant from C8166-grown stocks of virus containing 10^4 $TCID_{50}$ per milliliter. The inoculated macaques were compared to macaques inoculated with parental pathogenic $SHIV_{KU\text{-}1bMC33}$ and those inoculated with $SHIV_{TM}$ as previously described (Stephens et al., 2002; Hout et al., 2005). The animals were housed in the AAALAC-approved animal facility at the University of Kansas Medical Center. Heparinized blood was collected weekly for the first 4 weeks, then at 2 week intervals for the next month, and thereafter at monthly intervals.

Assays for circulating $CD4^+$ T cells

Alterations in the levels of $CD4^+$ lymphocytes after experimental inoculations were monitored sequentially by FACS analysis (Becton Dickinson). T lymphocyte subsets were labeled with OKT4 (CD4; Ortho Diagnostics Systems, Inc), SP34 (CD3; Pharmingen), or FN18 (CD3; Biosource International) monoclonal antibodies. T lymphocyte subsets from a normal uninfected macaque were always performed at the same time as inoculated macaques as a control for the FACS analysis.

Processing of tissue samples at necropsy

At the time of euthanasia, all animals in this study were anesthetized by administration of 10 mg/kg ketamine (IM) followed by an intravenously administration of sodium phenobarbital at 20–30 mg/kg. A laparotomy was performed and the animal exsanguinated by aortic canulation and perfused with 1 l of cold Ringer's saline. All aspects of the animal studies were performed according to the institutional guidelines for animal care and use at the University of Kansas Medical Center. Lymphoid tissues (lymph nodes, spleen, and thymus) and non-lymphoid tissues (brain, heart, kidneys, liver, lungs, pancreas, small intestine) were obtained and aliquots of tissue

snap frozen for DNA and RNA assays. Portions of lymphoid tissues were immersed in HBSS to quantify levels of infectious virus in tissues.

Sequence analysis of the vpu gene

The *vpu* was amplified from several tissue DNA samples taken at necropsy to examine the structure of *vpu*. For amplification of the *vpu*, we used oligonucleotide primers 5′-CCTAGACTAGAGCCCTGGAAGCATCC-3′ (sense) and 5′-GTACCTCTGTATCATATGCTTTAGCAT-3′ (antisense), which are complementary to nucleotides 5845–5870 and 6393–6420 of the HIV-1 (HXB2) genome (Ratner et al., 1985), respectively. One microgram of genomic DNA was used in the PCR with Taq DNA polymerase and the conditions described above. For the second round of amplification, we used oligonucleotide primers 5′-TTAGGCATCTCCTATGGCAGGAAGAAG-3′ (sense) and 5′-CACAAAATAGAGTGGTGGTTGCTTCCT-3′ (antisense), which are complementary to nucleotides 5956–5984 and 6386–6413 of the HIV-1 (HXB2) genome (Ratner et al., 1985), respectively. The conditions for amplification were identical to those described above. For sequence analysis, the PCR products from three separate PCRs were separated by electrophoresis in a 1% agarose gel, isolated, and each PCR reaction directly sequenced. Cycle sequencing reactions using the BigDye Terminator Cycle Sequencing Ready Reaction Kit with AmpliTaq DNA polymerase, FS (PE Applied Biosystems, Foster City, CA) and sequence detection were conducted with an Applied Biosystems 377 Prism XL automated DNA sequencer and visualized using the ABI Editview program. Sequences were compared to the intact sequences from $SHIV_{KU\text{-}1bMC33}$. Sequences showing differences were confirmed by molecularly cloning the PCR fragments into pGEM-T EZ vector followed by sequencing as described above.

PCR amplification of viral sequence from tissues

SHIV gag

DNA extracted from the visceral organs and different regions of the CNS as previously described (McCormick-Davis et al., 2000) was used to amplify viral *gag* sequences. The oligonucleotides used for the first round of amplification were 5′-GATGGGCGTGAGAAACTCCGTCTT-3′(sense) and 5′-CCTCCTCTGCCGCTAGATGGTGCTGTTG-3′ (antisense) corresponding to the regions 1052–1075 and 1423–1450 of the $SIV_{mac}239$ *gag* gene, respectively (Regier and Desrosiers, 1990). The nested $SIV_{mac}239$ primers used were 5′-GTTGAAGCATGTAGTATGGGCAGC-3′ (sense) and 5′-CACCACTAGGTGTCTCTGCACTATCTG-3′ (antisense) which are complementary to bases 1142–1165 and 1356–1382 of $SIV_{mac}239$, respectively.

Long terminal repeat circles

We examined tissue DNA samples for the presence of 2-LTR circular DNA (Zazzi et al., 1997; Teo et al., 1997; Sharkey and Stevenson, 2001; Sharkey et al., 2000). DNA isolated from visceral organs and 12 regions of the brain was analyzed for the presence of 2-LTR circular forms of DNA as previously described (McCormick-Davis et al., 2000). The oligonucleotides used in the first round were 5′-CCTCCTGTGCCTCATCTGATACATTTAC-3′ (U5 region) and 5′-ATTTCGCTCTGTATTCAGTCGCTCTGC-3′ (U3 region), which correspond to bases 10,335 to 10,361 and 180 to 153 of the SHIV genome, respectively. The PCR amplification was performed using the following conditions: denaturation at 92 °C for 1 min, annealing at 55 °C for 1 min, and primer extension at 72 °C for 3 min. One microliter of the first PCR product was used as a template for a second amplification using the same conditions. The oligonucleotides primers used for the second round were 5′-TTGGGTATCTAATTCCTGGTCCTGAG-3′ (U5 region) and 5′-AGGTTCTCTCCAGCACTAGCAGGTAGAGC-3′ (U3 region; opposite strand; 456), which correspond to bases 10,389 to 10,417 and 120 to 95 of the SHIV genome, respectively. The predicted product of the 2-LTR PCR product is 361 base pairs.

Analysis of virus loads in macaques

PCR-ICA

The virus loads in the CNS and lymphoid tissues were determined using a quantitative PCR assay modified from a PCR-infected cell assay previously described (Joag et al., 1994; Stephens et al., 1998). In this assay, 1 μg of total cellular DNA isolated from tissues was subjected to a series of 10-fold dilutions such that samples contained from 100 ng to 10 fg (less than one copy of chromosomal DNA). These samples were used in nested PCR reactions that amplified either the β-actin gene of the cell (a single copy gene) or the *gag* gene from $SHIV_{KU1bMC33}$. Amplification of either gene using the primers previously described was shown to detect one of the copy of each gene (Joag et al., 1994). Thus, amplification of the β-actin gene determined the number of genome equivalents in each sample, whereas amplification with the gag primers determined the number of viral copies per number of genome equivalents. The values were expressed as the number of viral copies per 10^6 genome equivalents.

Plasma virus loads

Plasma viral RNA loads were determined on RNA extracted from 500 μl of EDTA-treated plasma. Virus was pelleted and RNA extracted using the Qiagen viral RNA kit (Qiagen, Valencia, CA). RNA samples were analyzed by real-time RT-PCR using *gag* primers and a 5′FAM and 3′TAMRA labeled Taqman probe that was homologous to the SIV *gag* gene as previously described (Hofmann-Lehmann et al., 2000). Standard curves were prepared using a series of six 10-fold dilutions of viral RNA of known concentration. The sensitivity of the assay was 100 RNA equivalents per milliliter. Samples were analyzed in triplicate and the number of RNA equivalents was calculated per milliliter of plasma.

Acknowledgments

The work reported here is supported by NIH grants AI51981 and AA13845 to E.B.S. The anti-Vpu serum and the HeLa CD4$^+$ cell line were kindly provided by the NIH AIDS Research and Reference Reagent Program. We thank members of the KUMC Biotechnology Support Facility for their assistance with the sequence analysis and oligonucleotide synthesis.

References

Barlow, K.L., Ajao, A.O., Clewley, J.P., 2003. Characterization of a novel simian immunodeficiency virus (SIVmonNG1) genome sequence from a mona monkey (*Cercopithecus mona*). J. Virol. 77, 6879–6888.

Cohen, E.A., Terwilliger, E.F., Sodroski, J.G., Haseltine, W.A., 1988. Identification of a protein encoded by the *vpu* gene of HIV-1. Nature 334, 532–534.

Cordes, F.S., Kukol, A., Forrest, L.R., Arkin, I.T., Sansom, M.S., Fischer, W.B., 2001. The structure of the HIV-1 Vpu ion channel: modelling and simulation studies. Biochim. Biophys. Acta 1512, 291–298.

Cordes, F.S., Tustian, A.D., Sansom, M.S., Watts, A., Fischer, W.B., 2002. Bundles consisting of extended transmembrane segments of Vpu from HIV-1: computer simulations and conductance measurements. Biochemistry 41, 7359–7365.

Courgnaud, V., Salemi, M., Pourrut, X., Mpoudi-Ngole, E., Abela, B., Auzel, P., Bibollet-Ruche, F., Hahn, B., Vandamme, A.M., Delaporte, E., Peeters, M., 2002. Characterization of a novel simian immunodeficiency virus with a vpu gene from greater spot-nosed monkeys (*Cercopithecus nictitans*) provides new insights into simian/human immunodeficiency virus phylogeny. J. Virol. 76, 8298–8309.

Courgnaud, V., Abela, B., Pourrut, X., Mpoudi-Ngole, E., Loul, S., Delaporte, E., Peeters, M., 2003. Identification of a new simian immunodeficiency virus lineage with a vpu gene present among different cercopithecus monkeys (*C. mona*, *C. cephus*, and *C. nictitans*) from Cameroon. J. Virol. 77, 12523–12534.

Etemad-Moghadam, B., Sun, Y., Nicholson, E.K., Fernandes, M., Liou, K., Gomila, R., Lee, J., Sodroski, J., 2000. Envelope glycoprotein determinants of increased fusogenicity in a pathogenic simian–human immunodeficiency virus (SHIV-KB9) passaged in vivo. J. Virol. 74, 4433–4440.

Ewart, G.D., Sutherland, T., Gage, P.W., Cox, G.B., 1996. The Vpu protein of human immunodeficiency virus type 1 forms cation-selective ion channels. J. Virol. 70, 7108–7115.

Ewart, G.D., Mills, K., Cox, G.B., Gage, P.W., 2002. Amiloride derivatives block ion channel activity and enhancement of virus-like particle budding caused by HIV-1 protein Vpu. Eur. Biophys. J. 31, 26–35.

Ewart, G.D., Nasr, N., Naif, H., Cox, G.B., Cunningham, A.L., Gage, P.W., 2004. Potential new anti-human immunodeficiency virus type 1 compounds depress virus replication in cultured human macrophages. Antimicrob. Agents Chemother. 48, 2325–2330.

Fischer, W.B., Sansom, M.S., 2002. Viral ion channels: structure and function. Biochim. Biophys. Acta 1561, 27–45.

Fujita, K., Omura, S., Silver, J., 1997. Rapid degradation of CD4 in cells expressing human immunodeficiency virus type 1 Env and Vpu is blocked by proteasome inhibitors. J. Gen. Virol. 78, 619–625.

Goldsmith, M.A., Warmerdam, M.T., Atchison, R.E., Miller, M.D., Greene, W.C., 1995. Dissociation of the CD4 down-regulation and viral infectivity enhancement functions of human immunodeficiency virus type 1 Nef. J. Virol. 69, 4112–4121.

Gomez, L.M., Pacyniak, E., Mulcahy, E.R., Flick, M., Gomez, M., Nerrient, E., Ayouda, A., Santiago, M., Hahn, B., Stephens, E.B., 2005. Vpu mediated CD4 down-regulation and degradation is conserved among highly divergent SIV_{cpz} strains. Virology 335, 46–60.

Gonzalez, M.E., Carrasco, L., 2001. Human immunodeficiency virus type 1 VPU protein affects Sindbis virus glycoprotein processing and enhances membrane permeabilization. Virology 279, 201–209.

Gonzalez, M.E., Carrasco, L., 2003. Viroporins. FEBS Lett. 552, 28–34.

Grice, A.L., Kerr, I.D., Sansom, M.S., 1997. Ion channels formed by HIV-1 Vpu: a modelling and simulation study. FEBS Lett. 405, 299–304.

Hay, A.J., Zambon, M.C., Wolstenholme, A.J., Skehel, J.J., Smith, M.H., 1986. Molecular basis of resistance of influenza A viruses to amantadine. J. Antimicrob. Chemother. 18, 19–29.

Henkel, J.R., Weisz, O.A., 1998. Influenza virus M2 protein slows traffic along the secretory pathway. pH perturbation of acidified compartments affects early Golgi transport steps. J. Biol. Chem. 273, 6518–6524.

Henkel, J.R., Popovich, J.L., Gibson, G.A., Watkins, S.C., Weisz, O.A., 1999. Selective perturbation of early endosome and/or trans-Golgi network pH but not lysosome pH by dose-dependent expression of influenza M2 protein. J. Biol. Chem. 274, 9854–9860.

Hofmann-Lehmann, R., Swenerton, R.K., Liska, V., Leutenegger, C.M., Lutz, H., McClure, H.M., Ruprecht, R.M., 2000. Sensitive and robust one-tube real-time reverse transcriptase-polymerase chain reaction to quantify SIV RNA load: comparison of one- versus two-enzyme systems. AIDS Res. Hum. Retroviruses 16, 1247–1257.

Hout, D.R., Mulcahy, E.R., Pacyniak, E., Gomez, L.M., Gomez, M., Stephens, E.B., 2004a. Vpu: A multifunctional protein that enhances the pathogenesis of human immunodeficiency virus type 1. Cur. HIV-1 Res. 2, 255–270.

Hout, D.R., Gomez, M.L., Pacyniak, E., Mulcahy, E.R., Gomez, L.M., Jackson, M., Flick, M., Fegley, B., McCormick, C., Wisdom, B.J., Culley, N., Pinson, D.M., Powers, M., Wong, S.W., Stephens, E.B., 2004b. Fusion of the upstream vpu sequences to the env of simian human immunodeficiency virus (SHIVKU-1bMC33) results in the synthesis of two envelope precursor proteins, increased numbers of virus particles associated with the cell surface and is pathogenic for pig-tailed macaques. Virology 323, 91–107.

Hout, D.R., Gomez, M.L., Pacyniak, E., Gomez, L.M., Inbody, S.H., Mulcahy, E.R., Culley, N., Pinson, D.M., Powers, M.F., Wong, S.W., Stephens, E.B., 2005. Scrambling of the amino acids within the transmembrane domain of Vpu results in a simian–human immunodeficiency virus ($SHIV_{TM}$) that is less pathogenic for pig-tailed macaques. Virology 339, 56–69.

Huet, T., Cheynier, R., Meyerhans, A., Roelants, G., Wain-Hobson, S., 1990. Genetic organization of a chimpanzee lentivirus related to HIV-1. Nature 345, 356–359.

Joag, S.V., Stephens, E.B., Adams, R.J., Foresman, L., Narayan, O., 1994. Pathogenesis of SIVmac infection in Chinese and Indian rhesus macaques: effects of splenectomy on virus burden. Virology 200, 436–446.

Klimkait, T., Strebel, K., Hoggan, M.D., Martin, M.A., Orenstein, J.M., 1990. The human immunodeficiency virus type 1-specific protein vpu is required for efficient virus maturation and release. J. Virol. 64, 621–629.

Lamb, R.A., Pinto, L.H., 1997. Do Vpu and Vpr of human immunodeficiency virus type 1 and NB of influenza B virus have ion channel activities in the viral life cycles? Virology 229, 1–11.

Lopez, C.F., Montal, M., Blasie, J.K., Klein, M.L., Moore, P.B., 2002. Molecular dynamics investigation of membrane-bound bundles of the channel-forming transmembrane domain of viral protein U from the human immunodeficiency virus HIV-1. Biophys. J. 83, 1259–1267.

McCormick-Davis, C., Dalton, S.B., Hout, D.R., Singh, D.K., Berman, N.E., Yong, C., Pinson, D.M., Foresman, L., Stephens, E.B., 2000. A molecular clone of simian–human immunodeficiency virus ($\Delta vpuSHIV_{KU\text{-}1bMC33}$) with a truncated, non-membrane-bound vpu results in rapid CD4$^+$ T cell loss and neuroAIDS in pig-tailed macaques. Virology 272, 112–126.

Okada, A., Miura, T., Takeuchi, H., 2001. Protonation of histidine and histidine–tryptophan interaction in the activation of the M2 ion channel from influenza a virus. Biochemistry 40, 6053–6060.

Pacyniak, E., Gomez, M.L., Mulcahy, E.R., Jackson, M.J., Hout, D.R., Wisdom, B.J., Stephens, E.B., 2005. Identification of a region within the cytoplasmic domain of the subtype B Vpu protein of human immunodeficiency virus type 1 (HIV-1) that is responsible for retention in the Golgi complex and its absence in the Vpu protein from subtype C HIV-1. AIDS Res. Hum. Retroviruses 21, 379–394.

Park, S.H., Mrse, A.A., Nevzorov, A.A., Mesleh, M.F., Oblatt-Montal, M., Montal, M., Opella, S.J., 2003. Three-dimensional structure of the channel-

forming trans-membrane domain of virus protein "u" (Vpu) from HIV-1. J. Mol. Biol. 333, 409–424.

Paul, M., Jabbar, M.A., 1997. Phosphorylation of both phosphoacceptor sites in the HIV-1 Vpu cytoplasmic domain is essential for Vpu-mediated ER degradation of CD4. Virology 232, 207–216.

Ratner, L., Haseltine, W., Patarca, R., Livak, K.J., Starcich, B., Josephs, S.F., Doran, E.R., Rafalski, J.A., Whitehorn, E.A., Baumeister, K., et al., 1985. Complete nucleotide sequence of the AIDS virus, HTLV-III. Nature 313, 277–284.

Regier, D.A., Desrosiers, R.C., 1990. The complete nucleotide sequence of a pathogenic molecular clone of simian immunodeficiency virus. AIDS Res. Hum. Retroviruses 6, 1221–1231.

Sakaguchi, T., Leser, G.P., Lamb, R.A., 1996. The ion channel activity of the influenza virus M2 protein affects transport through the Golgi apparatus. J. Cell Biol. 133, 733–747.

Sansom, M.S., Forrest, L.R., Bull, R., 1998. Viral ion channels: molecular modeling and simulation. Bioessays 20, 992–1000.

Schubert, U., Henklein, P., Boldyreff, B., Wingender, E., Strebel, K., Porstmann, T., 1994. The human immunodeficiency virus type 1 encoded Vpu protein is phosphorylated by casein kinase-2 (CK-2) at positions Ser52 and Ser56 within a predicted alpha–helix–turn–alpha–helix–motif. J. Mol. Biol. 236, 16–25.

Schubert, U., Ferrer-Montiel, A.V., Oblatt-Montal, M., Henklein, P., Strebel, K., Montal, M., 1996a. Identification of an ion channel activity of the Vpu transmembrane domain and its involvement in the regulation of virus release from HIV-1-infected cells. FEBS Lett. 398, 12–18.

Schubert, U., Bour, S., Ferrer-Montiel, A.V., Montal, M., Maldarelli, F., Strebel, K., 1996b. The two biological activities of human immunodeficiency virus type 1 Vpu protein involve two separable structural domains. J. Virol. 70, 809–819.

Schubert, U., Anton, L.C., Bacik, I., Cox, J.H., Bour, S., Bennink, J.R., Orlowski, M., Strebel, K., Yewdell, J.W., 1998. CD4 glycoprotein degradation induced by human immunodeficiency virus type 1 Vpu protein requires the function of proteasomes and the ubiquitin-conjugating pathway. J. Virol. 72, 2280–2288.

Sharkey, M.E., Stevenson, M., 2001. Two long terminal repeat circles and persistent HIV-1 replication. Curr. Opin. Infect. Dis. 14, 5–11.

Sharkey, M.E., Teo, I., Greenough, T., Sharova, N., Luzuriaga, K., Sullivan, J.L., Bucy, R.P., Kostrikis, L.G., Haase, A., Veryard, C., Davaro, R.E., Cheeseman, S.H., Daly, J.S., Bova, C., Ellison III, R.T., Mady, B., Lai, K.K., Moyle, G., Nelson, M., Gazzard, B., Shaunak, S., Stevenson, M., 2000. Persistence of episomal HIV-1 infection intermediates in patients on highly active anti-retroviral therapy. Nat. Med. 6, 76–81.

Singh, D.K., Griffin, D.M., Pacyniak, E., Jackson, M., Werle, M.J., Wisdom, B., Sun, F., Hout, D.R., Pinson, D.M., Gunderson, R.S., Powers, M.F., Wong, S.W., Stephens, E.B., 2003. The presence of the casein kinase II phosphorylation sites of Vpu enhances the $CD4^+$ T cell loss caused by the simian–human immunodeficiency virus $SHIV_{KU\text{-}IbMC33}$ in pig-tailed macaques. Virology 313, 435–451.

Stephens, E.B., McClure, H.M., Narayan, O., 1995. The proteins of lymphocyte- and macrophage-tropic strains of simian immunodeficiency virus are processed differently in macrophages. Virology 206, 535–544.

Stephens, E.B., Mukherjee, S., Sahni, M., Zhuge, W., Raghavan, R., Singh, D.K., Leung, K., Atkinson, B., Li, Z., Joag, S.V., Liu, Z.Q., Narayan, O., 1997. A cell-free stock of simian–human immunodeficiency virus that causes AIDS in pig-tailed macaques has a limited number of amino acid substitutions in both SIVmac and HIV-1 regions of the genome and has offered cytotropism. Virology 231, 313–321.

Stephens, E.B., Sahni, M., Leung, K., Raghavan, R., Joag, S.V., Narayan, O., 1998. Nucleotide substitutions in the long terminal repeat are not required for development of neurovirulence by simian immunodeficiency virus strain mac. J. Gen. Virol. 79, 1089–1100.

Stephens, E.B., McCormick, C., Pacyniak, E., Griffin, D., Pinson, D.M., Sun, F., Nothnick, W., Wong, S.W., Gunderson, R., Berman, N.E., Singh, D.K., 2002. Deletion of the *vpu* sequences prior to the *env* in a simian–human immunodeficiency virus results in enhanced Env precursor synthesis but is less pathogenic for pig-tailed macaques. Virology 293, 252–261.

Strebel, K., Klimkait, T., Martin, M.A., 1988. A novel gene of HIV-1, *vpu*, and its 16-kilodalton product. Science 241, 1221–1223.

Takeuchi, H., Okada, A., Miura, T., 2003. Roles of the histidine and tryptophan side chains in the M2 proton channel from influenza A virus. FEBS Lett. 552, 35–38.

Tang, Y., Zaitseva, F., Lamb, R.A., Pinto, L.H., 2002. The gate of the influenza virus M2 proton channel is formed by a single tryptophan residue. J. Biol. Chem. 277, 39880–39886.

Teo, I., Veryard, C., Barnes, H., An, S.F., Jones, M., Lantos, P.L., Luthert, P., Shaunak, S., 1997. Circular forms of unintegrated human immunodeficiency virus type 1 DNA and high levels of viral protein expression: association with dementia and multinucleated giant cells in the brains of patients with AIDS. J. Virol. 71, 2928–2933.

Tiganos, E., Friborg, J., Allain, B., Daniel, N.G., Yao, X.J., Cohen, E.A., 1998. Structural and functional analysis of the membrane-spanning domain of the human immunodeficiency virus type 1 Vpu protein. Virology 251, 96–107.

Wang, C., Lamb, R.A., Pinto, L.H., 1995. Activation of the M2 ion channel of influenza virus: a role for the transmembrane domain histidine residue. Biophys. J. 69, 1363–1371.

Wray, V., Kinder, R., Federau, T., Henklein, P., Bechinger, B., Schubert, U., 1999. Solution structure and orientation of the transmembrane anchor domain of the HIV-1-encoded virus protein U by high-resolution and solid-state NMR spectroscopy. Biochemistry 38, 5272–5282.

Yao, X.J., Garzon, S., Boisvert, F., Haseltine, W.A., Cohen, E.A., 1993. The effect of vpu on HIV-1-induced syncytia formation. J. Acquired Immune Defic. Syndr. 6, 135–141.

Zazzi, M., Romano, L., Catucci, M., Venturi, G., De Milito, A., Almi, P., Gonnelli, A., Rubino, M., Occhini, U., Valensin, P.E., 1997. Evaluation of the presence of 2-LTR HIV-1 unintegrated DNA as a simple molecular predictor of disease progression. J. Med. Virol. 52, 20–25.